



OPEN ACCESS

EDITED BY

Chaojin Lu,
University of Miami, United States

REVIEWED BY

Zhengjian Xu,
Chongqing University of Science and
Technology, China
Zhongheng Sun,
Yangtze University, China
Fuyun Cong,
China University of Petroleum (East China),
China

*CORRESPONDENCE

Jie Li
✉ ljie@cug.edu.cn

RECEIVED 23 October 2024

ACCEPTED 10 December 2024

PUBLISHED 06 February 2025

CITATION

Li J, Cao Z, Geng F, Yang S, Sha X, Lan M,
Wang S, Lu Y, Lu Y, Tang D, Zhang Z and
Hao F (2025) The geometry evolution of Early
Paleozoic carbonate platform in the
southwestern Tarim Basin, China: evidence
from sequence stratigraphic analysis and
seismic forward modeling.
Front. Mar. Sci. 11:1515497.
doi: 10.3389/fmars.2024.1515497

COPYRIGHT

© 2025 Li, Cao, Geng, Yang, Sha, Lan, Wang,
Lu, Lu, Tang, Zhang and Hao. This is an open-
access article distributed under the terms of
the [Creative Commons Attribution License
\(CC BY\)](https://creativecommons.org/licenses/by/4.0/). The use, distribution or reproduction
in other forums is permitted, provided the
original author(s) and the copyright owner(s)
are credited and that the original publication
in this journal is cited, in accordance with
accepted academic practice. No use,
distribution or reproduction is permitted
which does not comply with these terms.

The geometry evolution of Early Paleozoic carbonate platform in the southwestern Tarim Basin, China: evidence from sequence stratigraphic analysis and seismic forward modeling

Jie Li^{1,2*}, Zicheng Cao³, Feng Geng³, Suju Yang³, Xuguang Sha³,
Mingjie Lan³, Shenghou Wang⁴, Yongchao Lu², Yangbo Lu²,
Daqing Tang², Zhao Zhang⁵ and Fang Hao⁶

¹Hubei Key Laboratory of Oil and Gas Exploration and Development in Hubei Province, China University of Geosciences, Wuhan, China, ²Key Laboratory of Tectonics and Petroleum Resources, China University of Geosciences, Wuhan, China, ³Sinopec Northwest Oil Field Company, Urumqi, China, ⁴Geophysical Research Institute, China Oilfield Services Limited, Tianjin, China, ⁵School of Petroleum Engineering, Guangdong University of Petrochemical Technology, Maoming, China, ⁶School of Geosciences, China University of Petroleum, East China, Qingdao, China

Deciphering the evolution of spatial geometry of carbonate platforms in deeply buried successions is still a challenge due to the low resolution of seismic data and the constraints of drilling wells. In this study, by combining a seismic forward model, we systematically delineated the external morphology and internal architecture of seismic reflection and established a depositional model of a carbonate platform. The Lower Paleozoic strata display the high-amplitude reflection in the Lower-Middle Cambrian interval and the low-amplitude reflection in the Upper Cambrian-Middle Ordovician interval. The high-amplitude reflection interval thins or wedges out towards the center of the present Southwest Depression section, and thickens to the north and south. Inside of the high-amplitude interval, the seismic reflection terminated at the top reflector. Seismic forward modeling was performed to examine the validity of possible hypothetical models in the studied area. The modeling results show that the simulated stratigraphic patterns are comparable to a ramp or depression geometry which is well fit to the characteristics of actual seismic reflections. Such a ramp or depression geometry is built upon the changes in sea level and climate during the Cambrian period. This study emphasizes the potential of the integration of sequence stratigraphic analyses and seismic forward modeling as a seismic workflow for retrieving the stratigraphic architecture and platform geometry.

KEYWORDS

ultra-deep, wedge, retrogradation, progradation, high-amplitude reflection, thickness, Cambrian, Ordovician

1 Introduction

1.1 Seismic interpretation

Seismic data provide an opportunity to construct stratigraphical architecture at a large scale (Zeng et al., 1998; Zeng and Hentz, 2004; Rankey, 2017). Seismic interpretation at the shelf break (margin and slope) is crucial for the sedimentary and stratigraphical framework as the rapid changing of slope steepness causes a large variation in accommodation versus sedimentation and thus sharp facies transition (Vecsei and Sanders, 1997; Rinke-Hardekopf et al., 2018). Many economically recoverable oil and gas reservoirs are located around the shelf breaks, which neighbor basinal shales with hydrocarbon source potential (Gao and Fan, 2015; Grant et al., 2018). Shelf breaks could be identified with diagnostic characteristics of time thickness, external geometry and internal architecture on seismic profiles, such as wedges, fans, and reflection terminations (Cathro et al., 2003; Rankey, 2017; Zeng et al., 2022; Riera et al., 2023). In the past five decades, seismic facies analyses based on external geometry and internal architecture were very effective for uncovering basin architecture, sedimentary models, platform evolution, and even global sea level changes, climate events, ocean currents, and so on (Saller et al., 2004; Colpaert et al., 2007; Tian et al., 2015; Seyedmehdi et al., 2016; Espejel et al., 2021; Qin et al., 2022; Zeng et al., 2022; Riera et al., 2023).

Seismic investigations on modern or shallowly buried carbonate shelves provide opportunities to observe and understand marine sediment transport and accumulation at shelf breaks (Feary and James, 1995; Cathro et al., 2003; Principaud et al., 2015; Mulder et al., 2017; Rankey, 2017; Rinke-Hardekopf et al., 2018; Tesch et al., 2018; Qin et al., 2022), and models were developed to predict economic targets around the world (Lee and Watkins, 1998; Playton and Kerans, 2015; Gong et al., 2016; Cunha et al., 2021; Zeng et al., 2022). Great progress has been achieved in the offshore deep-water areas (Janson et al., 2011; Espejel et al., 2021). However, challenges are encountered in deeply buried (below 6000 m) marine successions. Highly compacted carbonate rocks with high velocity and evaporite screening high-frequency signals lower the resolution of seismic profiles (Janson et al., 2007; Grant et al., 2018; Zeng et al., 2011; 2022). Interference from multiple reflections are also rampant. Additionally, few drilling wells are available for well-seismic calibration. Seismic studies on deeply buried cases were rarely reported. Under such conditions, seismic forward modeling appeared to be a necessary tentation (Wu et al., 2018; He et al., 2019; Zeng et al., 2022).

1.2 Geometry of carbonate platforms in the Tarim Basin

Geological understanding of the Lower Paleozoic marine strata in the Tarim Basin has to a large extent been driven by energy exploration (Jin and Wang, 2004; He et al., 2005; Wang et al., 2014). However, most exploration activities have been distributed at the periphery of the Manjar Depression which acts as the main

hydrocarbon kitchen of the northern Tarim Basin (Zhang et al., 2014; Li et al., 2015; Zhu et al., 2016; He et al., 2023). The southwestern Tarim Basin remains less explored because of a perceived lack of hydrocarbon sources speculated from previous 2D seismic investigations (Chen et al., 2015; Wu et al., 2016; Yang et al., 2017; Zhang et al., 2019; Zhu et al., 2021a; Gao et al., 2022; Yuan et al., 2022). Additionally, the Cambrian strata are too deep (>9000 m) to reach, and no wells are available to identify the presence of black shales. Recently, new organic geochemical analyses of oil produced from the Ordovician period in the Yubei oil field indicate that 60% of the contribution was sourced from the Lower Cambrian marine sequence (Cao et al., 2021). This reignited exploration interests and led to a re-examination of the seismic profiles (Feng et al., 2015; Cui et al., 2018; Tian et al., 2020; Geng et al., 2023).

Due to well calibration and paleo-topographic constraints, there are significant uncertainties in the seismic interpretations of the lower Paleozoic strata in the southwestern Tarim region. Currently, at least three geometry hypotheses have been proposed (Figure 1).

Hypothesis A: Uplift (Figure 1A)

The uplift hypothesis suggests that the thinnest part of the high-amplitude reflection interval represents a paleo-uplift with NW-SE strike during the Early Cambrian (Chen et al., 2015; Feng et al., 2015; Liu et al., 2016; Zhang et al., 2019; Wu et al., 2021; Zhu et al., 2021a; Yuan et al., 2022). The high-amplitude interval thickening northward and southward resulted from the Upper Ediacaran-Lower Cambrian onlap on the basement. During the late Ediacaran and early Cambrian periods, the southern side of the paleo-uplift dipped into the ancient Kunlun Ocean, while the northern side developed an intra-continental shallow hollow between two paleo-uplifts. By the Middle Cambrian, this paleo-uplift was submerged, as was the Bachu Uplift. The available accommodation controls the stratal thickness, which is at its thinnest on the paleo-uplift.

Hypothesis B: Ramp (Figure 1B)

The ramp hypothesis suggests that the Lower Paleozoic strata were deposited on a south-dipping ramp (Cui et al., 2016, 2018; Tian et al., 2020; Wei et al., 2021; Geng et al., 2023). In the late Ediacaran, the Maigaiti Slope and Bachu Uplift sections were exposed, and clastic sediments were delivered southward from the exposed metamorphic basement to the Southwestern Depression section. The deltaic coastal deposition exhibits wedge-shaped seismic reflections. By the Early Cambrian, a major transgression drowned the whole southwestern Tarim Basin and is characterized by marine transgressive deposits above the Ediacaran strata and the metamorphic basement. In the Early to Middle Cambrian, fine-grained sediments and evaporites were deposited in the northern shallow- and back-ramp environments with relatively low sea levels, displaying high-amplitude low-frequency reflections. In the southern part, the basin and deep ramp were farther away from the shallow carbonate factory, and thus the stratal thickness decreases southward.

Hypothesis C: Depression (Figure 1C)

The depression hypothesis suggests that there was an intracraton depression at the center of the Southwestern

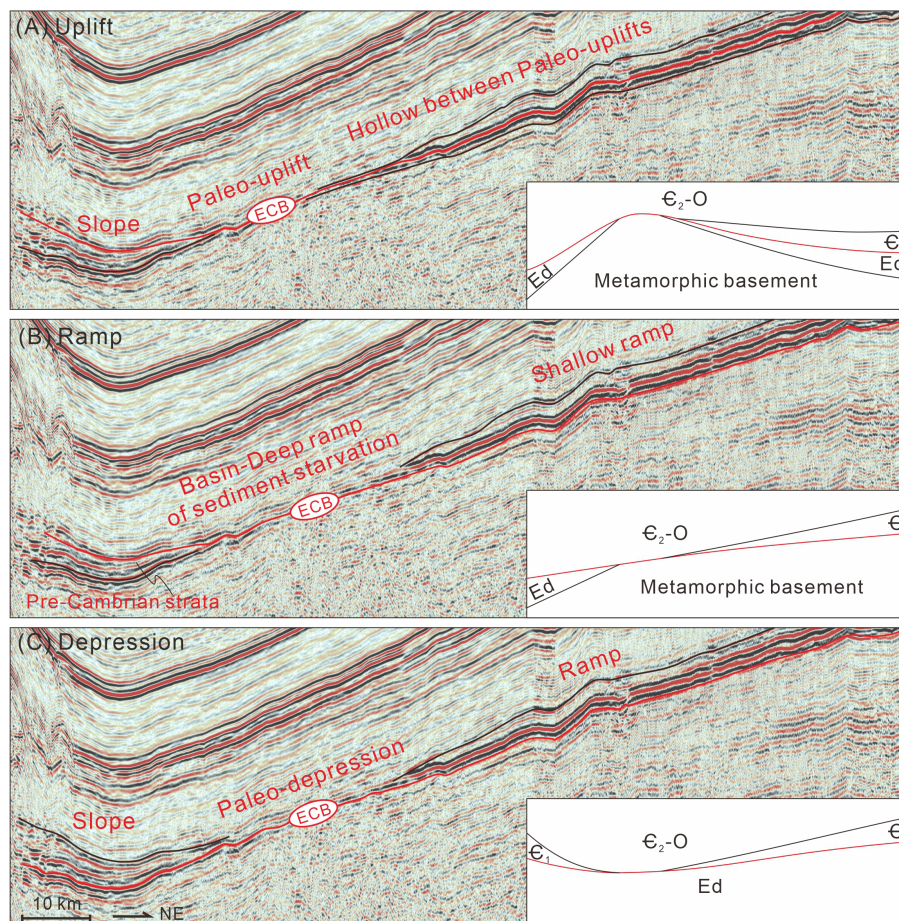


FIGURE 1

Three interpretations of the geometry of the Lower Paleozoic strata in the southwestern Tarim Basin, with the red line labelling the seismic event of Ediacaran-Cambrian interface on the seismic profile and schematic cartoons of hypothetical paleo-landscapes at the lower right corners. (A) the Uplift interpretation, (B) the Ramp Interpretation, (C) the Depression Interpretation. Ed, Ediacaran; ϵ_1 , Lower Cambrian; ϵ_2 , Middle Cambrian; O, Ordovician, ECB, Ediacaran-Cambrian Boundary.

Depression section, and a paleo-topographic high at the southern edge (Gao and Fan, 2015). The wedge-shaped reflection body represents the slope fan or wedge on the slope toe and paleo-depression. While on the Maigaiti Slope and Bachu Uplift sections, a carbonate ramp developed southward-dipping. The deep ramp has a lower sediment supply rate and thus thinner strata towards the paleo-depression.

In this study, we endeavor to elucidate the stratigraphic framework and platform geometry of the underexplored Lower Paleozoic strata in the southwestern Tarim Basin. With 2D seismic profiles of the southwestern Tarim Basin, a correlation with seismic profiles from more explored adjacent areas was utilized to identify the estimated target intervals. Subsequently, based on reflection amplitude, external geometry, and internal architecture, we found common seismic features. Based on the three interpretations of geometry above, we proposed four hypotheses for stratal stacking patterns based on sequence stratigraphic interpretations. Lithology and velocity models were built and then seismic forward modeling was conducted to examine the validity of the hypothetical geometries. Ultimately, sedimentary models were constructed and

controls on platform geometry evolution were analyzed for the Ordovician-Cambrian strata in the southwestern Tarim Basin.

2 Geological settings

2.1 Geography and tectonics

The Tarim Basin is the largest superimposed basin (560,000 km²) in northwestern China, bounded by the Tianshan Mountains to the north, the Kunlun Mountains to the south and southwest, and the Altyn Mountains to the southeast (Jia, 1997). The Tarim Block consists of two Precambrian basements, i.e., the South and North Tarim terranes (top left of Figure 2; Liou et al., 1996; Yin and Nie, 1996; Zusa and Yin, 2017). The amalgamation between the two terranes occurred in the Early-Middle Neoproterozoic era and built up the paleo-high Central Tarim suture zone (Xu et al., 2013; Wu et al., 2018; Yang et al., 2018; Zhao et al., 2021). This paleo-topography controlled the sedimentary dipping of the subsequent Early Paleozoic on both sides of the Central Tarim suture zone.

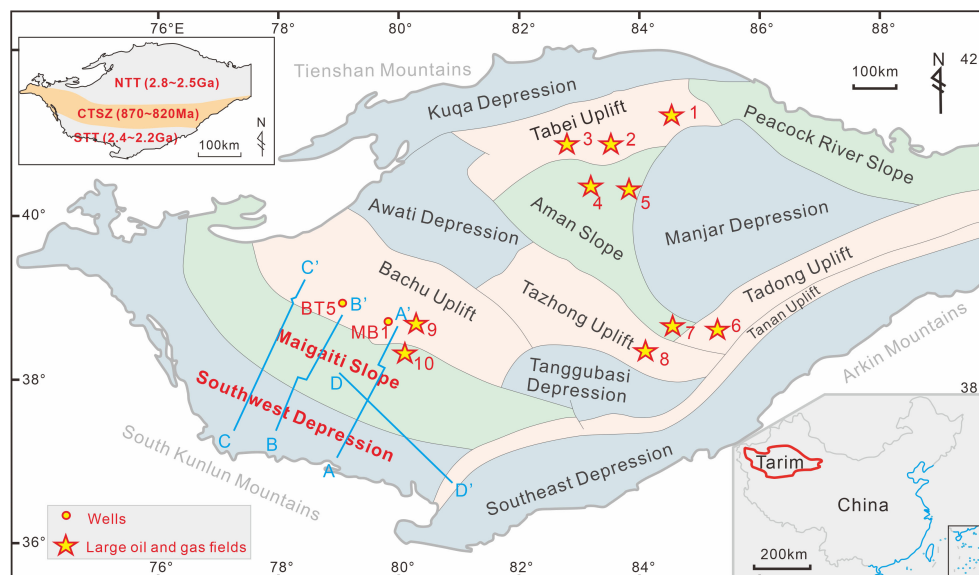


FIGURE 2

Geological settings and structural sections of the Tarim Basin and distribution of 2D seismic profiles of this study in the southwestern Tarim Basin. The small map in the upper left corner shows the basements of the Tarim Basin and their respective geological ages: North Tarim Terrance (NTT), South Tarim Terrane (STT), and Central Tarim Suture/Terrane Zone (CTSZ) (Xu et al., 2023). The small map in the lower right corner exhibits the geographical location of the Tarim Basin. Large oil and gas fields: 1 = Lungu Oil Field, 2 = Tahe Oil and Gas Field, 3 = Halahatang Oil Field, 4 = Shunbei Oil Field, 5 = Fuman Oil Field, 6 = Gucheng Gas Field, 7 = Shunnan Gas Field, 8 = Tazhong Oil and Gas Field, 9 = Hotan River Gas Field, 10 = Yubei Oil and Gas Field.

Then, prolonged tectonic movements and subsidence broke the whole Tarim Basin into structural depressions, slopes, and uplifts: Kuqa, Awati, Manjar, Tanggubasi, Southeastern and Southwest depressions; Aman, Peacock, and Maigaiti slopes; Tabei, Bachu, Tazhong, Tadong, and Tanan uplifts (Figure 2; Jia, 1997). Our study area is the southwestern Tarim Basin, including the Southwest Depression and Maigaiti Slope sections.

Since the Cambrian period, the southwestern Tarim Basin was located at the passive continental margin under an extensional tectonic condition. Until the middle Ordovician period, the ancient Kunlun Ocean closed and thrust to the southwestern Tarim Basin. From the late Ordovician to the Carboniferous period, the southwestern Tarim Basin was continuously tectonically compressed and an exposed uplift was recognized due to no marine sedimentation at the southern edge of Tarim Basin. In the Cenozoic period, the southwestern Tarim Basin experienced structural adjustment, its northern part uplifted rapidly, and the southern part subsided, creating the present structural landscape of north-high and south-low (Yue and Luo, 2019).

2.2 Stratigraphy

The southwestern Tarim Basin evolution has four stages: (i) rifted basin, Cryogenian; (ii) rifted to aulacogen basin, Early Ediacaran; (iii) aulacogen basin, Late Ediacaran; (iv) stable craton basin, Cambrian to Middle Ordovician (Tian et al., 2020; Wei et al., 2021). Different basin types exerted control over the sediment types and stratal stacking patterns. The Lower Paleozoic strata in the

southwestern Tarim Basin primarily consist of marine deposits including the Cambrian carbonate-evaporite successions and Ordovician carbonate successions (Figure 3). During the early Cambrian, the southwestern Tarim Basin experienced tectonic extension at the western margin of the Laurentia supercontinent. During the middle Ordovician, the southern margin experienced tectonic transformation from extension to compression. This tectonic transformation turned the stable craton basin into an intra-continental depression basin, simultaneously causing the exhumation of the lower Paleozoic strata (Figure 3; Zhang et al., 2019; Zhao et al., 2021). The closure of the ancient Kunlun Ocean and buildup of the Kunlun orogenic belt intensified the relief differences between the uplifts and depressions. During the extensional period, four supersequences (SSQ1-SSQ4) developed from the Cambrian to the Middle Ordovician, coinciding with the global long-term sea level rise (Figure 3). During the early compressional period, one supersequence (SSQ5) developed with the late Ordovician long-term sea level falling (Figure 3).

SSQ1 started from the earliest Cambrian transgression, and ended at Stage 4. The transgressive hemicycle is the Yurtus Formation (E_{1y}), with its base and top corresponding to seismic events T90 and T85. On the paleo-highs within the Tarim Basin, such as the Bachu-Tazhong region, the E_{1y} did not deposit. In contrast, the paleo-lows such as the Tabei Uplift area, had a thick deposition of deep-water organic-rich shales and marls, contributing to the basin-scale hydrocarbon source. The regressive hemicycle comprises the Xiaerbulake (E_{1x}) and Wusongger (E_{1w}) Formations. In the Bachu-Tazhong region, the E_{1x} and E_{1w} consist of micritic dolostones bearing terrigenous

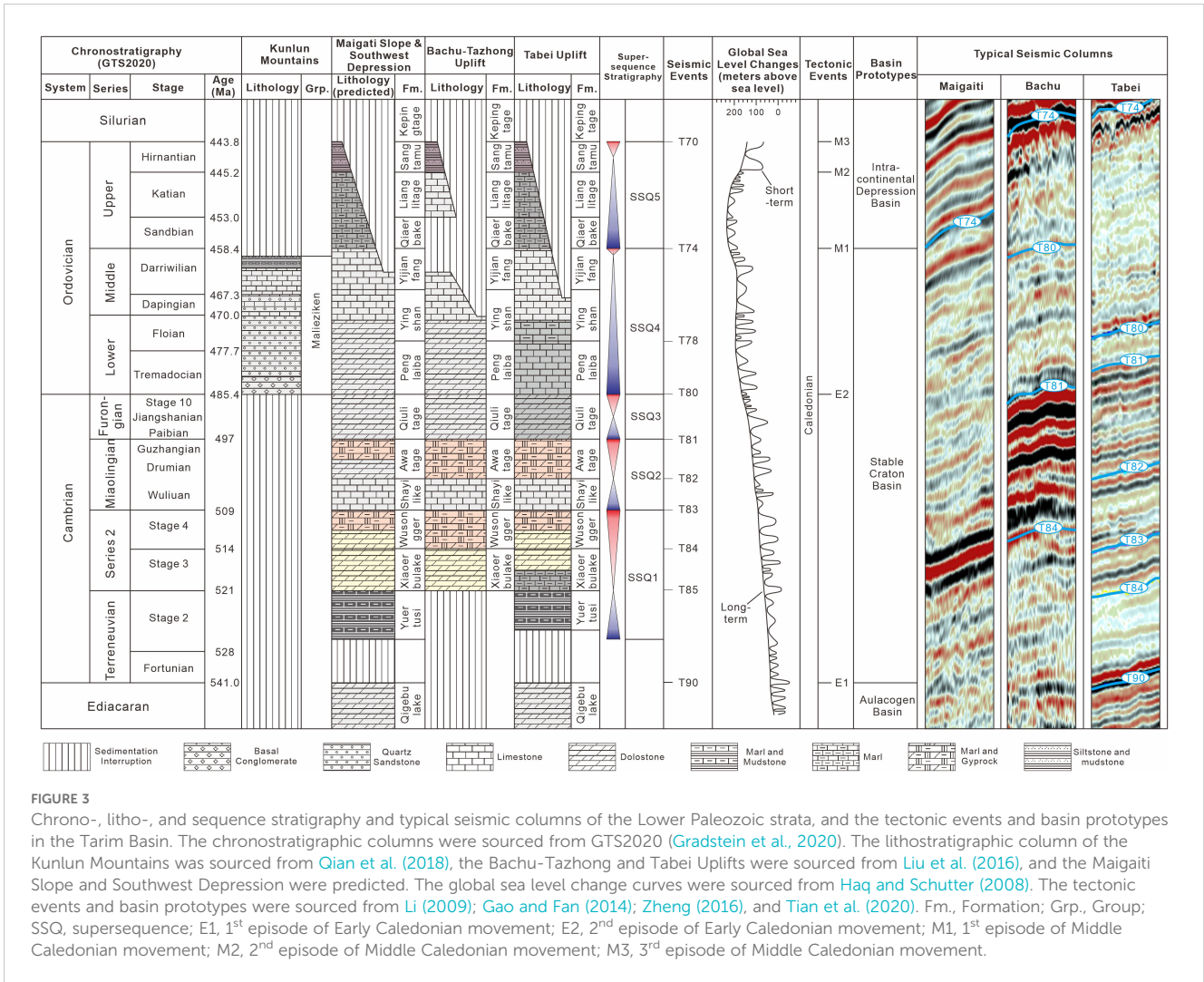


FIGURE 3

Chrono-, litho-, and sequence stratigraphy and typical seismic columns of the Lower Paleozoic strata, and the tectonic events and basin prototypes in the Tarim Basin. The chronostratigraphic columns were sourced from GTS2020 (Gradstein et al., 2020). The lithostratigraphic column of the Kunlun Mountains was sourced from Qian et al. (2018), the Bachu-Tazhong and Tabei Uplifts were sourced from Liu et al. (2016), and the Maigaiti Slope and Southwest Depression were predicted. The global sea level change curves were sourced from Haq and Schutter (2008). The tectonic events and basin prototypes were sourced from Li (2009); Gao and Fan (2014); Zheng (2016), and Tian et al. (2020). Fm., Formation; Grp., Group; SSQ, supersequence; E1, 1st episode of Early Caledonian movement; E2, 2nd episode of Early Caledonian movement; M1, 1st episode of Middle Caledonian movement; M2, 2nd episode of Middle Caledonian movement; M3, 3rd episode of Middle Caledonian movement.

quartz sand, stromatolite dolostones, and gypseous dolostones, representing tidal flat deposits. At the platform margin and slope facies belts in the Tabei Uplift area, the E_{1x} is composed of the lower muddy-limestone interval and the upper wacke- and pack-dolostone interval, while the E_{1w} consists of lower oolitic dolostones and upper gypsiferous and argillaceous dolostones. Considering the extensional tectonic setting, the paleo-topography in the southwestern Tarim Basin is inferred to be lower compared to the Bachu paleo-uplift. Therefore, in the southwestern Tarim Basin, SSQ1 probably comprises deep-water shales and marls, shallow tidal flat massive dolostones, and tidal flat gypsiferous and argillaceous dolostone from bottom to top (Figure 3). The top of SSQ1 is the seismic event T83, and the one between the E_{1x} and E_{1w} is T84.

SSQ2 corresponds to the Miaolingian Series, consisting of the Shayilik (E_{2s}) and Awatage (E_{2a}) Formations. The E_{2s} commonly consists of limestones in drilling wells and outcrops, representing the transgressive hemicycle, with its top corresponding to T82. In contrast, the E_{2a} typically comprises red mudstone, gypsum, and salt, indicating a regressive hemicycle, with its top corresponding to T81.

SSQ3 corresponds to the Furongian Series, composed of various white massive crystalline dolostones and microbialites in shallow subtidal environments. Small lithological variations within SSQ3 make it challenging to discern the transgressive and regressive semicycles, collectively referred to as the Qiulitage Group (E_{3q}), with its top being T80.

SSQ4 comprises the Penglaiba (O_{1p}), Yingshan (O_{1-2y}), and Yijianfang (O_{2y}) Formations. In the Bachu area, the O_{1p} and lower member of O_{1-2y} (O_{1-2y}¹) consist of thick-bedded massive dolostones, the upper member of O_{1-2y} (O_{1-2y}²) and O_{2y} consist of thick-bedded massive limestones, both of which are shallow subtidal carbonates. In the southwestern Tarim Basin, the Middle Ordovician underwent erosion to a different extent. The top of O_{1p} (T78) is not consistently clear in the Tarim Basin, while T74 at the top of SSQ4 is recognizable, with extensive unconformity and a significant lithological interface, making T74 the best seismic event for the Lower Paleozoic stratigraphic correlation. In the Kunlun Mountains, SSQ4 outcropped, as a deepening-upward sequence from the basal conglomerate, to quartz sandstone and then bioclastic limestone and finally black marls in a back-arc basin on the Mesoproterozoic metamorphic basement (Qian et al., 2018).

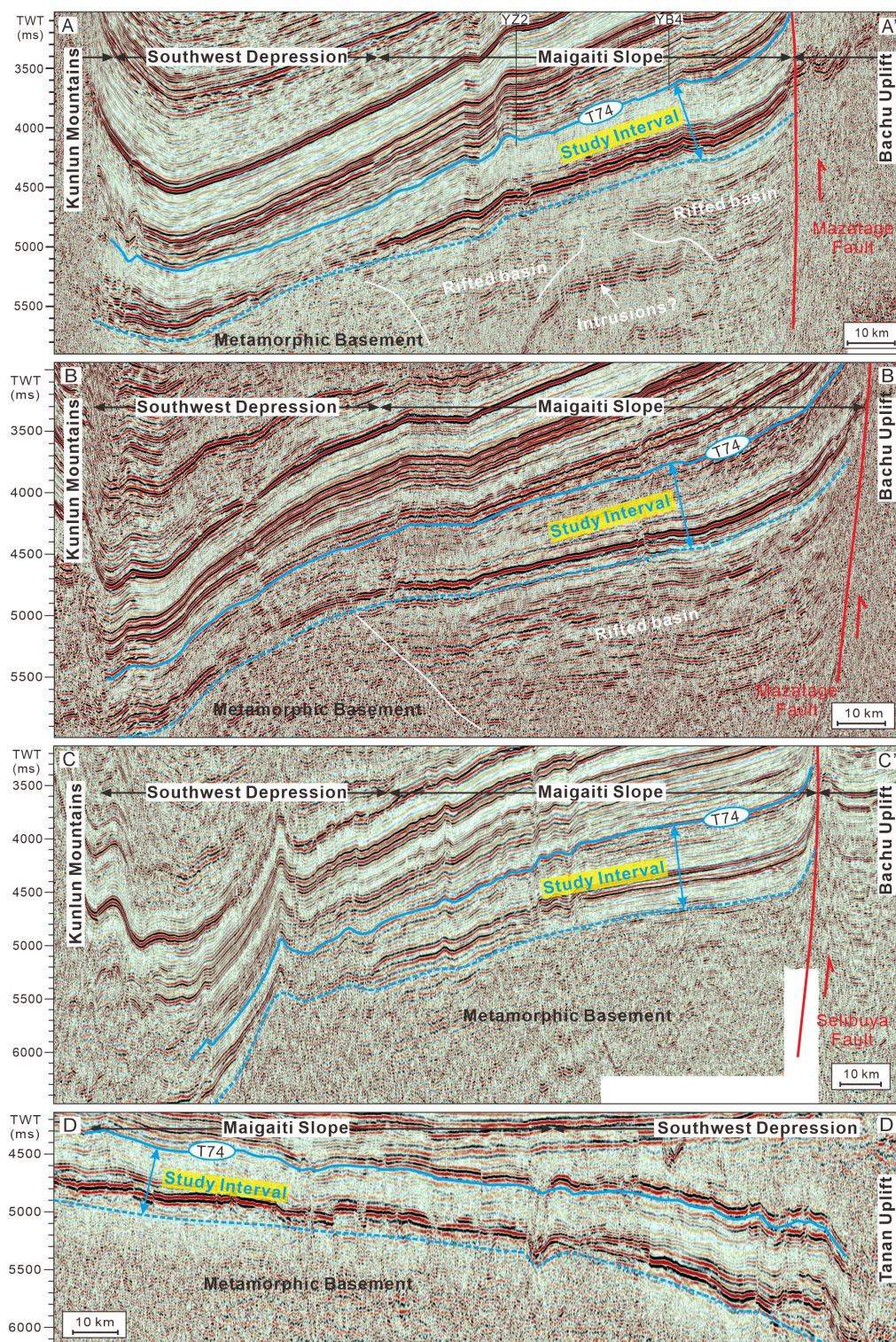
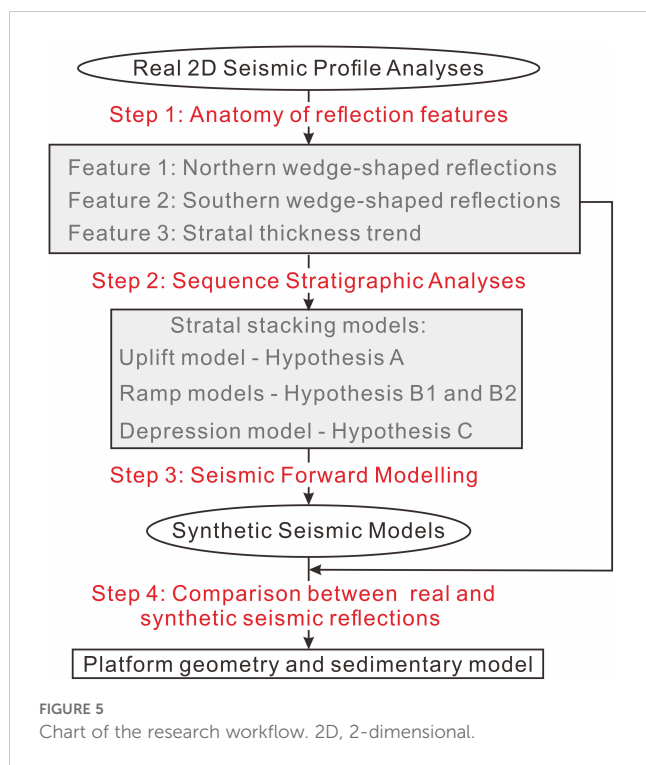


FIGURE 4
 Seismic profiles with the outlined study interval including the Middle-Lower Ordovician (below the T74 surface), Cambrian, and the uppermost of the Precambrian basement. The locations of these profiles are shown in the [Figure 1](#). (A–C) profiles are northeast-southwest oriented, and the (D) profile is northwest-southeast oriented. The T74 surface can be calibrated by wells in the Yubei Oil and Gas Field and the Bachu Uplift ([Gao et al., 2015](#); [Liu et al., 2016](#); [Yuan et al., 2022](#)).



SSQ5 represents the Upper Ordovician strata, deposited as a thick marine transgressive sequence above the T74 unconformity across the Tarim Basin. It comprises the Qiaerbake (O_{3q}), Lianglitage (O_{3l}), and Sangtamu (O_{3s}) Formations (mainly muddy and silty sediments). SSQ5 plays the role of a basin-scale seal for the Lower Paleozoic hydrocarbon system.

2.3 Major seismic events

The Tabei Uplift area, with abundant deep drillings and high-resolution 3D seismic surveys, provided the opportunity to identify critical seismic interfaces in the Lower Paleozoic (Zeng et al., 2011, 2022; Lu et al., 2017). The top of the Middle Ordovician exhibits a high-amplitude, serrated seismic event (T74). The massive limestone in the Middle Ordovician and massive dolostone in the Upper Cambrian-Lower Ordovician primarily display low-amplitude subparallel reflectors. T80 between the Cambrian and Ordovician is marked by a high-amplitude reflector (Figure 3, right side). Frequent alternations of mudstone, gyprock, salt, and carbonate layers in the Middle-Lower Cambrian produce laterally continuous high-amplitude reflectors (T81-T84). T90, between the lowermost Cambrian shales and the Ediacaran dolostones, displays laterally continuous high-amplitude reflectors. In conclusion, the stratigraphic interval between T74 and T90, the object of our study, appears as four intervals of parallel, high-amplitude reflections (T74, T80, T81-84, T90) sandwiched between three intervals of low-amplitude, subparallel reflections (Figure 3, right side).

In the Bachu Uplift area, the top of Middle Ordovician (T74) and laterally continuous high-amplitude subparallel reflectors in the Middle-Lower Cambrian (T81-T84) can be correlated with those in

the Tabei Uplift area (Lv et al., 2010; Yang et al., 2017). However, T80 disappeared because of the lack of lithological difference between the Upper Cambrian and Lower Ordovician. The absence of the lowermost Cambrian shale deposits and the slight impedance contrast between the overlying Cambrian shallow dolostone and metamorphic basement make the T90 interface seismically indiscernible. Therefore, in the Bachu Uplift area, only the T74, T81, and T84 seismic events can be regionally traced (Figure 3, right side).

In the Southwestern Tarim Basin, the fewest identifiable seismic events are present. This is due to the lack of deep well constraints and a scarcity of laterally continuous high-amplitude reflectors traceable in seismic profiles (Figure 3). Only the T74 can be constrained by two wells, without karst-featured reflections (YZ2 and YB4 in Figure 4A).

3 Methods

3.1 Database and workflow

The 2D seismic profiles were collected from SINOPEC. Four representative profiles are displayed in this study (Figures 2, 4). These seismic profiles are all post-stack migration sections and were interpreted using Landmark Openworks2005. The A-A' profile, the most analyzed by previous publications, was selected for detailed genetic stratigraphic analyses and seismic forward modeling as it has well-imaged internal architecture and reflection terminations.

The complete workflow of this study involved four steps (Figure 5): (1) anatomy of the common reflection features, (2) sequence stratigraphic interpretation, (3) seismic forward modeling, (4) and comparison between actual and synthetic seismic reflections.

The external morphology and internal architecture were analyzed and three common reflection features were summarized (Step 1). We then interpreted these reflection features based on the principles of sequence stratigraphy. Four stratigraphic models of stratal stacking patterns were enumerated under three types of platform geometry (Step 2).

Furthermore, based on previously published sedimentary models of geometry hypotheses, four 2D lithological models along the sedimentation trend were constructed for subsequent velocity models. The same parameters for window size, sources, and signal were adopted in all models (Table 1) to conduct seismic forward modeling in Tesseral software (Step 3).

Finally, the modeling results were compared with the A-A' profile. The external geometry and internal architecture of the high-amplitude reflection interval were checked and three features were the focus of comparison. In particular, reflection amplitude and

TABLE 1 Parameters for seismic forward modeling.

Window size		Source		Signal	
Length	135 km	Shot point number	2701	Wavelet	Ricker
Width	6.25 km	Receiver number	2700	Frequency	15 Hz
Area	843.75 km ²	Offset	25m	Variance	2D Elastic

TABLE 2 P-wave velocity and density in velocity models.

Lithofacies type	P-wave velocity	Density
Limestone	6,500	2,900
Marl limestone	4,286	2,742
Dolostone	4,667	2,800
Argillaceous dolostone	4,418	2,780
Sandstone	5,125	2,750
Shale and siltstone	3,313	2,450
Shaly evaporates	3,937	2,212
Gneiss	5,850	2,750

terminations with sequence stratigraphic significance were carefully examined (Step 4).

3.2 Seismic forward modeling

Our seismic forward modeling focused on the wedge-shaped morphology and reflection terminations within the high-amplitude reflections. The lithological distributions were adopted from previous published sedimentary models of the uplift, ramp, and depression hypotheses (Chen et al., 2015; Gao and Fan, 2015; Cui et al., 2016).

The low-amplitude interval displays massive parallel-subparallel reflections. It suggests no sharp lithological variation, although some predictable migration of facies belts had occurred in the Ordovician strata (Gao and Fan, 2015; Wei et al., 2021; Zhu et al., 2021a). Therefore, the lithology of the low-amplitude intervals was simplified in our lithology models.

Eight lithological members have to be included in the lithological models. P-wave velocity and density values were then applied to turn the lithological models into velocity models (Table 2). Finally, seismic forward modeling results were produced and visualized.

4 Results

4.1 Vertical amplitude variation

The Middle-Upper Ordovician displays laterally continuous moderate-amplitude parallel reflectors, different from those of the Tabei and Bachu Uplift areas. Most seismic events cannot be traced from the Bachu Uplift, as reflections are significantly different across the Mazatage-Selibuya fault zone (Figures 4A–C; Gao et al., 2015). From the Lower Ordovician to the basement, the seismic profile primarily consists of low-amplitude chaotic to subparallel reflectors, intercalating with an interval of laterally continuous high-amplitude parallel reflections, possibly representing the Middle Cambrian evaporite sequences (T81) to the base of the Lower Cambrian shales (T90) (Lin et al., 2014; Cui et al., 2016; Geng et al., 2023).

The seismic profiles illustrate the structural boundaries of the southwestern Tarim Basin. Its southern margin is bordered by the Kunlun Mountains, the northern margin is bounded by the Mazatage-Selibuya deep-seated faults neighboring the Bachu Uplift (Figures 4A–C), and the eastern margin is bordered by the Yubei thrust belt (Figure 4D; Lin et al., 2015). The profiles exhibit a double-layer pattern, separated by the blue dashed line in Figure 4. Below the blue dashed line, pervasive chaotic reflections resemble those below T90 in the Bachu Uplift area. Local parallel-subparallel reflection bodies show a graben-like geometry. The interval above the blue dashed line displays laterally continuous parallel or subparallel reflection bodies with stable time thickness, indicating sedimentary strata within the stable post-rift basin. Thus, this double-layer pattern represents the transition from a rifted basin to a post-rift basin. Our study interval lies between the blue solid and dashed lines (Figure 4).

4.2 Lateral amplitude and continuity variation and terminations

The examined strata dip southward to the edge of the Kunlun Mountains. The northern part is seated on the Maigaiti Slope section, while the southern part is on the Southwest Depression section. The time thickness ranges from 3,500 ms at the northern edge to 6,000 ms at the southern edge. Along the northern edge, the top and bottom of the study interval are at depths of 3,200–3,700 ms and 3,900–4,400 ms respectively, and the time thickness is approximately 700 ms. Along the southern boundary, the top and bottom are at depths of approximately 5,200–5,800 and 5,900–6,500 ms, and the vertical time thickness is also approximately 500 ms. The thinnest time thickness (~400 ms) occurs at the center of the Southwest Depression section. Overall, the strata thin towards the center of the Southwest Depression section, and thicken to the north and south.

Specifically, the lower part of the study interval with high-amplitude reflections is only 100 ms at the center of the Southwest Depression section, and it thickens to 200 ms northward and 400 ms southward. This trend of stratal thickness coincides with that of the entire study interval (Figure 6A). A closer observation of the internal architecture of the high-amplitude interval reveals the difference between the north and south. At the north section, reflection amplitudes gradually increase northward, and a couple of new reflectors emerge with terminations on the uppermost wave trough of the high-amplitude interval (Figure 6B). At the south section, the number of high-amplitude reflectors increases southward, forming the wedge-shape reflection body, where all internal reflectors terminate at the second wave trough on the top of wedge (Figure 6C). A similar wedge-shaped reflection body is observed in the southeast edge (Figure 4D), whereas the upper part of the study interval, displaying low-amplitude subparallel reflections, has a consistent thickness (300 ms) (Figure 4). Thus, the north-south trend of stratal thickness of the studied interval seems primarily due to that of the lower part.

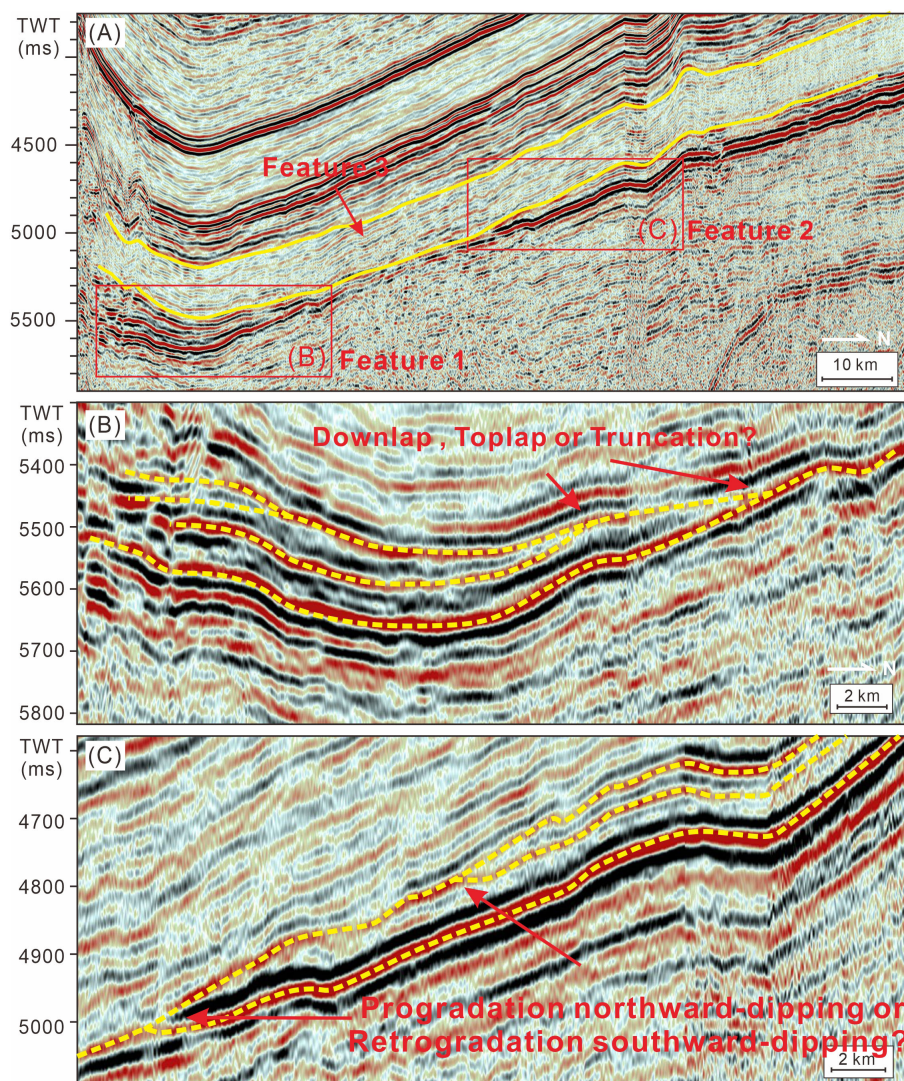


FIGURE 6

Two-dimensional seismic reflection features of the Ordovician and Cambrian strata in the southwestern Tarim Basin. (A) The seismic section was sourced from the A-A' profile with labelled and exaggerated wedge-shape reflection at the south side (B) and the north side (C).

From the above description of seismic profiles, three features can be summarized:

- Feature 1: Wedge-shaped high-amplitude reflections terminated at the second wave trough at the top of the southern section.
- Feature 2: Wedge-shaped high-amplitude reflections terminated at the uppermost wave trough in the northern section.
- Feature 3: Stratal thickness change in the study interval derived from the high-amplitude reflection interval thickening northwards and southwards while the low-amplitude reflection interval has a consistent thickness from south to north.

4.3 Seismic forward models

4.3.1 Lithological models

In the uplift model, only the south end of the paleo-uplift stays submarine at the latest Ediacaran. With the relative sea level dropping (SSQ0), individual foresets of coastal delta offlap and are prograded with upper sandstone and lower mudstone (Feature 1). The Early Cambrian marine transgression submerged the paleo-uplift, and a carbonate ramp north-dipping appeared on the north side of the paleo-uplift. Feature 2 was interpreted as two offlap points of the foresets when the sea level rose slowly or stayed the same (E_{1x} and E_{1w}). Each foreset bed is composed of lower argillaceous dolostone and upper dolostone (Figure 7A).

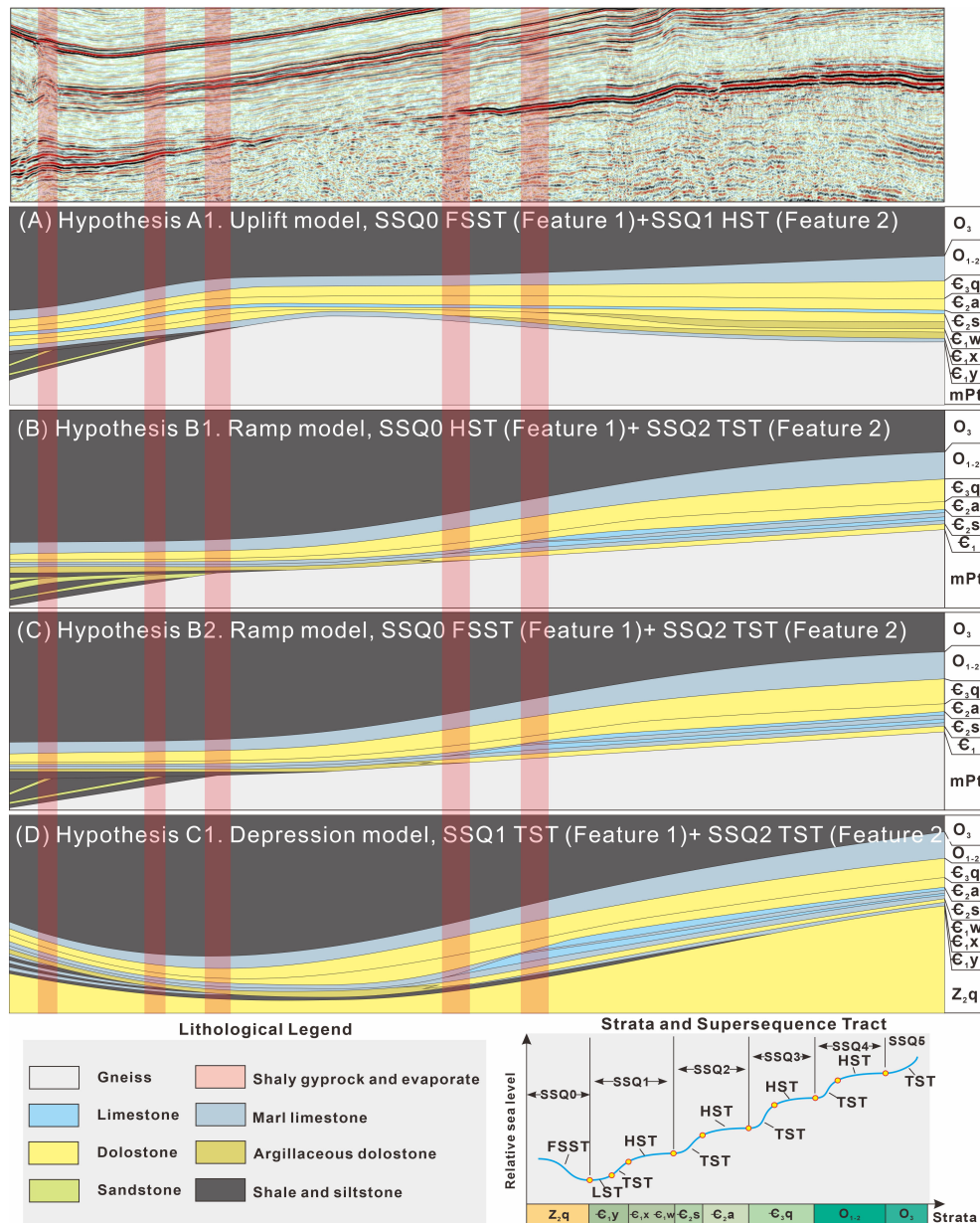


FIGURE 7
 Lithological models for the four hypotheses and the original seismic profile posted for comparison of the reflection terminations. **(A)** Lithological model of hypothesis A1, the uplift model, with the uppermost Ediacaran stratum (SSQ0) as FSST in the south and $\epsilon 1x-\epsilon 1w$ (SSQ1) progradation as HST in the north. **(B)** Lithological model of hypothesis B1, the ramp model, with the uppermost Ediacaran stratum (SSQ0) as HST in the south and $\epsilon 2s$ (SSQ2) retrogradation as TST in the north. **(C)** Lithological model of hypothesis B2, the ramp model, with the uppermost Ediacaran stratum (SSQ0) as FSST in the south and $\epsilon 2s$ (SSQ2) retrogradation as TST in the north. **(D)** Lithological model of hypothesis C1, the depression model, with the lowermost Cambrian $\epsilon 1y$ (SSQ1) retrogradation as TST in the south and $\epsilon 2s$ (SSQ2) retrogradation as TST in the north.

In the ramp model, due to the uncertainty of the sedimentary base level, Feature 1 can be interpreted as the offlapping falling-stage system tract (FSST) or the toplapping highstand system tract (HST) with the top sediment bypass. Whether FSST or HST, Feature 1 should be a clastic sand coast deposit with the proximal exposed metamorphic basement being the clastic source. The foresets in Feature 1 were formed during forced or normal regression and are composed of upper sandstone and lower mudstone. In contrast, Feature 2 can only be interpreted as retrograding and upstepping foresets as the ramp is south-

dipping during the Middle Cambrian transgression ($\epsilon 2s$) (Figures 7B, C).

In the depression model, both Feature 1 and Feature 2 are retrograding and upstepping foresets as the transgressive system tract (TST), because the arrangement direction of the reflection termination points is opposite to the depositional dip. At the paleotopographic low, the depression evolved from the Precambrian rift trough; while at the paleo-topographic high, the basements of the Lower Paleozoic should be Ediacaran marine dolostones rather than exposed metamorphic rocks (Figure 7D).

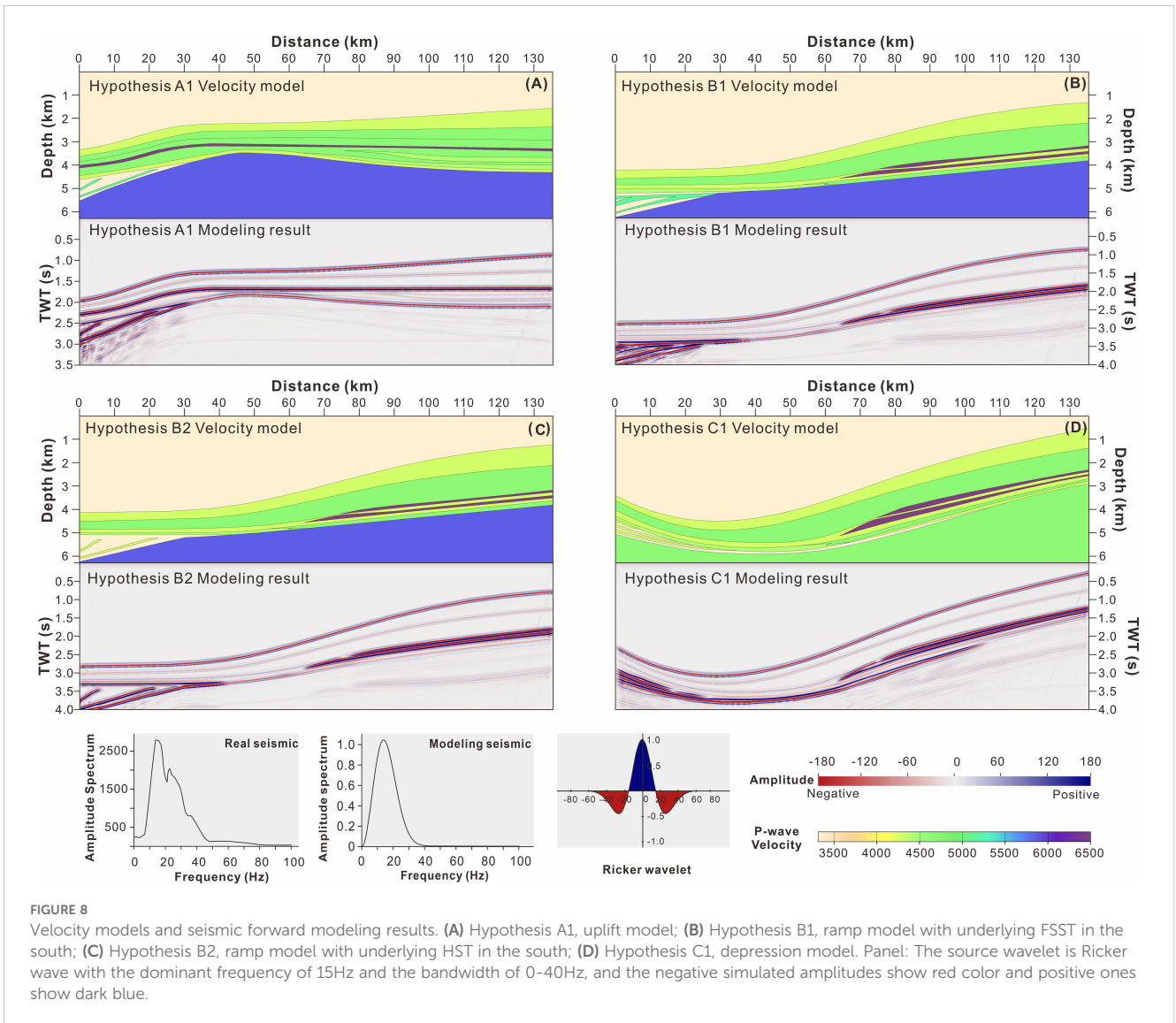


FIGURE 8 Velocity models and seismic forward modeling results. (A) Hypothesis A1, uplift model; (B) Hypothesis B1, ramp model with underlying FSST in the south; (C) Hypothesis B2, ramp model with underlying HST in the south; (D) Hypothesis C1, depression model. Panel: The source wavelet is Ricker wave with the dominant frequency of 15Hz and the bandwidth of 0-40Hz, and the negative simulated amplitudes show red color and positive ones show dark blue.

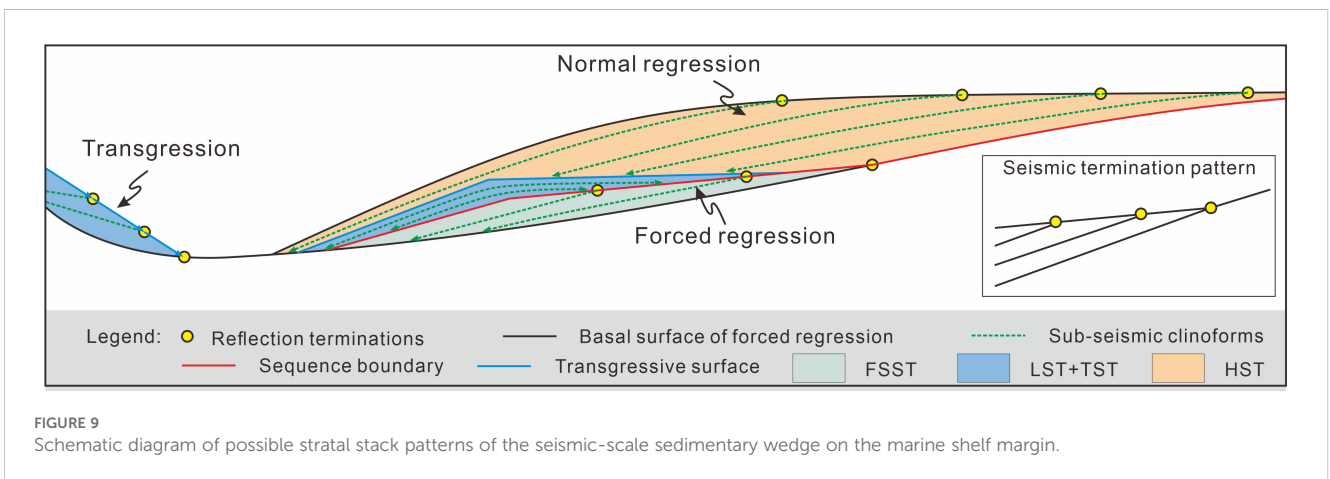


FIGURE 9 Schematic diagram of possible stratal stack patterns of the seismic-scale sedimentary wedge on the marine shelf margin.

4.3.2 Velocity models and simulated seismic models

We focused on the amplitudes and reflection terminations of the seismic forward modeling results and the alignment of the reflection termination points. In the four hypotheses, Feature 1 has three stratigraphic interpretations: FSST in Hypotheses A1 and B2 (Figures 8A, C), HST in Hypothesis B1 (Figure 8B), and TST in Hypothesis C1 (Figure 8D). The modeling reflection architectures of FSST and TST are consistent with the actual seismic profile with reflection terminating at the wave trough (Figure 6B). In contrast, the modeling reflectors of HST terminate at the wave peak (Figure 8B). Accordingly, Feature 1 could be a south-dipping FSST or a north-dipping TST. Feature 2 has two interpretations: HST in Hypothesis A1 (Figure 8A) and TST in the other three hypotheses (Figures 8B–D). The latter is consistent with the actual seismic profile, and the reflection termination points of the TST line are at the wave trough (Figure 6C); whereas those of the former HST line are at different reflectors (Figure 8A).

5 Discussion

5.1 Sequence stratigraphic interpretation of reflection architecture

The Lower Paleozoic sequence stratigraphy of the Tarim Basin has been extensively documented, based on outcrops, core samples, well logs, and high-resolution 3D seismic data (Yang et al., 2011; Zhao et al., 2011; Gao and Fan, 2014; Geng et al., 2023; Zhang et al., 2023). The number of third-order sequences within the Cambrian-

Ordovician strata was reported to be more than 30, significantly exceeding the number of seismic maximum lobes in the southwestern Tarim Basin. Consequently, the interpretation of third-order sequence stratigraphy on these 2D seismic profiles is impractical. The sequences analyzed in this study are second order, i.e., supersequences (SSQ1-4) (Figure 2). The terminology adopted in our sequence stratigraphic analyses follows the works of Hunt and Tucker (1992) and Catuneanu et al. (2009).

5.1.1 Interpretation of the wedge-shaped reflection body at the southern section (Feature 1)

The thickness variation of isochronous stratigraphic units is a function of available accommodation and sediment supply (Vail et al., 1977; Catuneanu et al., 2009). The shelf margin typically has the greatest thickness and then thickness decreases both landward and basinward due to the limited accommodation and low carbonate supply rate respectively, resulting in seismic wedges thinning towards both land and basin (Figure 9). Thus, the wedge shape could develop at either the proximal or distal part of the carbonate platform.

The internal reflectors of the wedges are parallel to the base of the wedge and terminate at the top wave trough (Figure 6B). Three scenarios have the potential to interpret this internal architecture. The first scenario is southward-prograding foresets during highstand normal regression (Normal Regression in Figure 9). The second scenario is southward-prograding oblique clinoforms during falling-stand forced regression (Forced Regression in Figure 9). The wedge shape of Feature 1 might display a proximal part of the foresets in the above two scenarios. The third scenario is

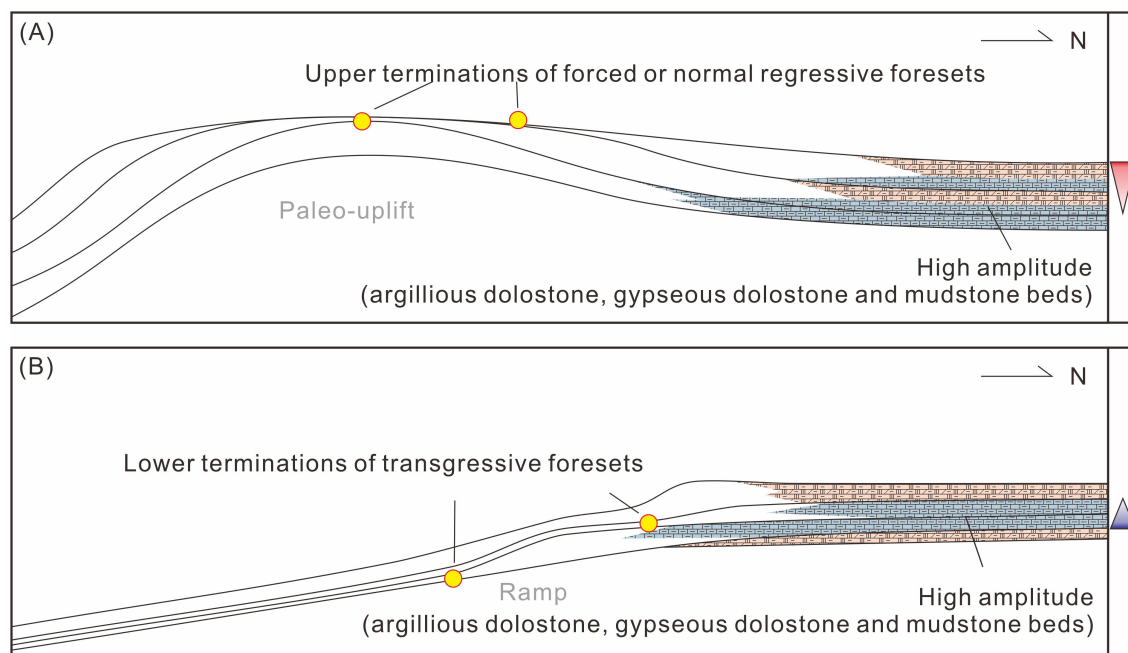


FIGURE 10

Two possible stratal stack patterns of strong amplitude reflections in Feature 2. (A) Terminations formed during a high-stand period, with marl limestone, mudstone, and gyprock beds deposited at the hollow between the hypothetical paleo-uplift and Bachu Uplift. (B) Terminations formed during marine transgression, with marl limestone, mudstone, and gyprock beds deposited at the lagoon inside of the platform.

retrograding foresets during marine transgression (Transgression in Figure 9). In this scenario, the wedge shape might exhibit the distal part of the foresets in the third scenario.

5.1.2 Interpretation of the wedge-shaped reflection body at the northern section (Feature 2)

The interpretation of Feature 2 also has uncertainties, because both northward- and southward-dipping paleo-topographies need to be considered. Classical sequence stratigraphy indicates that if the relative sea level rises slowly, stays, or falls and sediment supply exceeds the creation of accommodation, sediment would be transported from the shelf top and shed at the slope and basin (Vecsei and Sanders, 1997). In the uplift model, sedimentation dips northward (Figure 10A). The foresets are stacked with toplap terminations, and the bottomsets consist of marl limestone, mudstone, and evaporite beds displaying high amplitudes in the hollow or lagoon environment. With the filling of the hollow, the volume of low-amplitude foresets composed of shallow massive carbonates gradually decreases, while that of the bottomsets of the evaporitic and restricted lagoon gradually increases, creating high-amplitude reflections.

In the ramp and depression models, sedimentation dips southward (Figure 10B). When the relative sea level rises rapidly and the creation of accommodation exceeds the sediment supply, carbonate platforms have a strong tendency to defend their margins prior to ultimate backstepping, rather than gradually retreat landward as siliciclastics do (Schlager, 1998). In this case, the foresets retrograded with downlap terminations. In the proximal back-shoal environment, fine sediments composed of marl dolostone, gypseous dolostone, and mudstone beds display high-amplitude reflections. As a result, the number of high-amplitude reflectors increases towards the north, with the backstepping of the shelf margin and back-shoal belts during a second-order marine transgression.

5.1.3 Interpretation of the stratal thickness change (Feature 3)

The above interpretations of Features 1 and 2 explain the stratal thickness trend of the high-amplitude interval (Figures 4, 6) while the consistent thickness of the low-amplitude interval reveals that the platform pattern and sedimentary system were different from that of the high-amplitude interval.

Previous research studies suggested that the Ordovician sedimentary system continuously evolved from the Cambrian one (Gao and Fan, 2015; Liu et al., 2016; Zhang et al., 2019, 2023). Many wells on the Bachu Uplift and northern Maigaiti Slope section reached the Ordovician massive limestones and dolostones deposited from the shallow open-platform environment, while the Kandilik outcrop and W18 Well at the southern edge of the Southwest Tarim Basin have encountered Lower Ordovician shales and mudstones, indicating a deep environment (Gao and Fan, 2015; Liu et al., 2016). Between the shallow open platform and deep environment, many south-dipping clinofolds with sub-parallel, moderate-to-low-amplitude reflections exist, indicating

that the Ordovician platform evolved from the Cambrian ramp or depression. Sediment shedding could contribute to the filling of the slope and depression, and the Late Cambrian-Middle Ordovician tectonic denudation partially decreased the stratal thickness on the platform top. Finally, the Ordovician strata show a consistent thickness from north to south.

5.1.4 Sequence stratigraphic frameworks

The main challenge in establishing the sequence stratigraphic framework lies in the high-amplitude interval, due to the uncertainties in interpreting the geometry and internal architecture of seismic reflections (i.e., Features 1 and 2). Therefore, selecting reasonable combinations of different interpretations of Feature 1 and 2 is a necessary step toward an actual stratigraphic and sedimentary framework.

The top of the upper Ediacaran Qigebulak Formation (SSQ0) in the Tarim Basin is generally characterized by an unconformity surface. This indicates a significant basin-wide sea level fall in the late Ediacaran (He et al., 2010). Subsequently, in the early Paleozoic, three major transgressions occurred across the Tarim Basin. The first transgression took place during the early Cambrian (TST in SSQ1), the transgressive sequence containing black shales covered the upper Ediacaran carbonates (SSQ0) or even the metamorphic basement (Zhu et al., 2016). The second transgression, consisting of the Middle Cambrian massive carbonates (TST in SSQ2), was deposited on the Lower Cambrian evaporites and evaporitic dolostones (Geng et al., 2023). Rapid sea level fluctuations and consequent lithological changes are possibly responsible for the high-amplitude seismic reflections in the Early to Middle Cambrian sequences (SSQ1-2). The third transgression occurred in the Late Ordovician, with interlayered mudstones and marls deposited and continuous high-amplitude reflections above T74 displayed (Figure 4). From the Late Ordovician to the Middle Ordovician, the relative sea level was stable, producing thick massive carbonate beds (SSQ3-4) with low amplitudes. The amplitude difference between SSQ1-2 and SSQ3-4 has also been found in other regions of the Tarim Basin. Therefore, the chronological age of the high-amplitude reflections (Feature 1 and 2) can be roughly constrained to between the late Ediacaran and Middle Cambrian (SSQ0-SSQ2), while the low-amplitude reflections are approximately from the Late Cambrian to Middle Ordovician (SSQ3-4). Additionally, in the travel-time profile, the reflector at which the reflection terminations line up in Feature 1 is one wave-length lower than that of Feature 2, indicating that Feature 1 deposited before Feature 2. Taking the above together, we selected and constructed four possible processes for the stratal stacking in Features 1 and 2 (Figure 11).

In the uplift model, Feature 1 represents the FSST of SSQ0, while Feature 2 corresponds to the HST of either SSQ1 or SSQ2 (Figure 11A). Feature 1 is inferred to have formed during the late Ediacaran (SSQ0), when a significant sea level fall resulted in the deposition of deltaic wedges with truncation at the top at the shelf slope as FSST rather than HST. Moreover, SSQ1 and SSQ2 developed on the paleo-topographically higher Bachu Uplift without obvious exposed surfaces, indicating that the seawater had already drowned the entire study area without significant

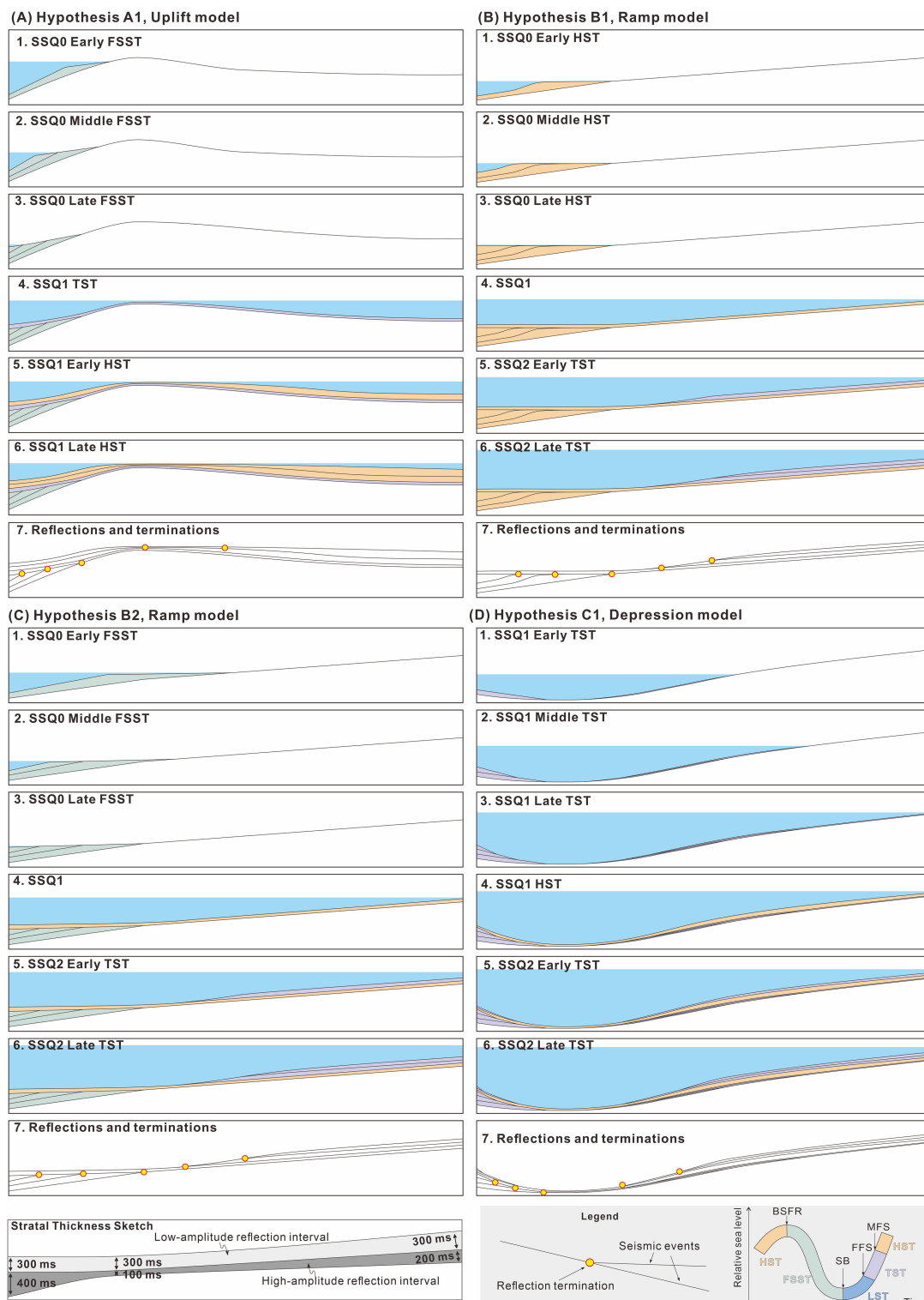


FIGURE 11
 Four possible interpretations of the stratal stack patterns based on sequence stratigraphic considerations for the architecture and terminations of the seismic wedge. **(A)** the Hypothesis A1 from the Uplift interpretation, **(B)** the Hypothesis B1 from the Ramp interpretation, **(C)** the Hypothesis B2 from the Ramp interpretation, **(D)** the Hypothesis C1 from the Depression interpretation. Left panel: thickness constrains for models. Right panel: symbol introduction and applied sequence stratigraphic terminology. FSST, falling-stage system tract; LST, lowstand system tract; TST, transgressive system tract; HST, highstand system tract; BSFR, basal surface of forced regression; SB, sequence boundary; FFS, first flooding surface; MFS, maximum flooding surface.

TABLE 3 Schematic diagram of Features 1 and 2 from the seismic forward modeling results matched with the actual seismic reflectors.

Hypothetic models		Feature 1		Feature 2	
Model No.	Land scape	Modeling result	Match	Modeling result	Match
A1	Uplift		Yes		No
B1	Ramp		No		Yes
B2	Ramp		Yes		Yes
C1	Depression		Yes		Yes

Red lines represent wave troughs and blue lines represent wave peaks. Notably, the reflection terminations in Features 1 and 2 all occur on the wave troughs.

falling, which did not allow truncation or toplap terminations in the paleo-topographically lower locations of Feature 1. During the regressive hemicycles of SSQ1 or SSQ2, a shallow carbonate factory was produced and prograded northward, creating oblique clinofolds with toplap terminations (Feature 2). We cannot definitively assign Feature 2 to either SSQ1 or SSQ2 based on the existing data. This uncertainty has a slight impact on the subsequent forward modeling results and the overall sedimentation model. In this study, we tentatively assigned Feature 2 to be SSQ1, otherwise, SSQ1 would be too thin (Figure 11A).

In the ramp model, Feature 1 represents the HST or FSST of SSQ0, while Feature 2 corresponds to the TST of SSQ2 (Figures 11B, C). The inference of Feature 1 as the FSST of SSQ0 has been detailed in the previous paragraph. The possibility can then be excluded that Feature 2 was born in SSQ1 based on two lines of indirect inference. First, the Yurtus Formation in the northern Tarim Basin is only 10–20 m thick (TST of SSQ1) on the platform, and reaches a maximum thickness of 75 m (LST plus TST of SSQ1) in the deepest basin environment (Gao et al., 2022). This suggests that the transgression of SSQ1 was rapid and starved of sediments. Thus, the thickness of Feature 2 (approximately 300 ms) does not match that of SSQ1. Second, if Feature 2 belonged to SSQ1, the outer zone of the backstepping margin should have experienced sediment starvation and downlapped directly on the top surface of SSQ0. However, the fact is that Feature 2 is ~50ms above Feature 1 by one reflector (Figure 6A). Therefore, our model reconstructed the sedimentation process so that, during the late Ediacaran period, deltaic deposition prograded southward in the present Southwest Depression area, with the relative sea level staying constant (HST in Figure 11B) or falling (FSST in Figure 11C). Meanwhile, a gentle slope dipping southward was exposed in the present Maigaiti Slope area. In the Early Cambrian, the entire study area was underwater and evolved into a carbonate ramp system. During the Middle Cambrian transgression, shallow marine carbonate factories backstepped and kept up with the rising sea level, while the deeper environments were starved of sediments,

creating a carbonate-rimmed platform that evolved from the preexisting ramp.

In the depression model, Feature 1 represents the TST of SSQ1, while Feature 2 corresponds to the TST of SSQ2 (Figure 11D). They resulted from two transgressions during the Early and Middle Cambrian respectively. It is important to note that the presence of sharp shelf margin breaks is necessary for the occurrence of seismic-scale carbonate platform backstepping transgressions (Cathro et al., 2003; Campbell, 2005; Kenter et al., 2005; Bover-Arnal et al., 2009; Playton and Kerans, 2015). A steep slope probably developed to the south of the ancient depression, while a gentle ramp developed to the north with no seismic-visible counterpart in Feature 1. During the Middle Cambrian marine transgression, the ramp evolved into a rimmed platform with buildups at the margin, resulting in seismic-visible backstepping retrogradation on the northern side of the depression.

5.2 Evaluation on the simulated seismic models

The reflection architecture of Features 1 and 2 in the four forward modeling results are simply sketched and compared with that of the actual seismic profile (Table 3). The forward modeling results of Hypotheses B2 and C1 match well with the actual seismic profile, while Hypotheses A1 and B1 do not match. Therefore, our forward modeling results suggest the ramp and depression models for the sedimentary framework and exclude the uplift model.

5.3 Platform evolution and controls

As discussed above, the sedimentation of the Lower Paleozoic strata was initiated on a ramp or an intracraton depression. The sedimentary trend is northeast-southwest, and the sedimentary models of the ramp and depression settings are very similar at the present Maigaiti Slope section on the northeast side (Figure 12). Here, the earliest Cambrian transgression (E_{1y}) occurred on a south-dipping ramp, which developed on an exposed metamorphic basement or a flat epeiric platform. The increase in available accommodation was very limited during the subsequent highstand period (E_{1x} and E_{1w}), which led to the large-scale migration of the sedimentary facies belt and the thinness of the Lower Cambrian strata. During the Middle Cambrian transgression (E_{2s}), the high aggradation potential of the carbonate high-energy facies belt built up the platform margin, turning the ramp into a rimmed platform. With the marginal buildup growing, the inner platform became more and more restricted and even evolved into an evaporative lagoon. From the Late Cambrian to the Middle Ordovician (E_{3q} – O_{2y}), the sedimentary facies belts did not differentiate significantly, and the sedimentary environments switched between open platforms and restricted platforms alternatively (Figure 12).

The difference between the ramp and depression models occurs in the Southwest Depression section. In the ramp model, the

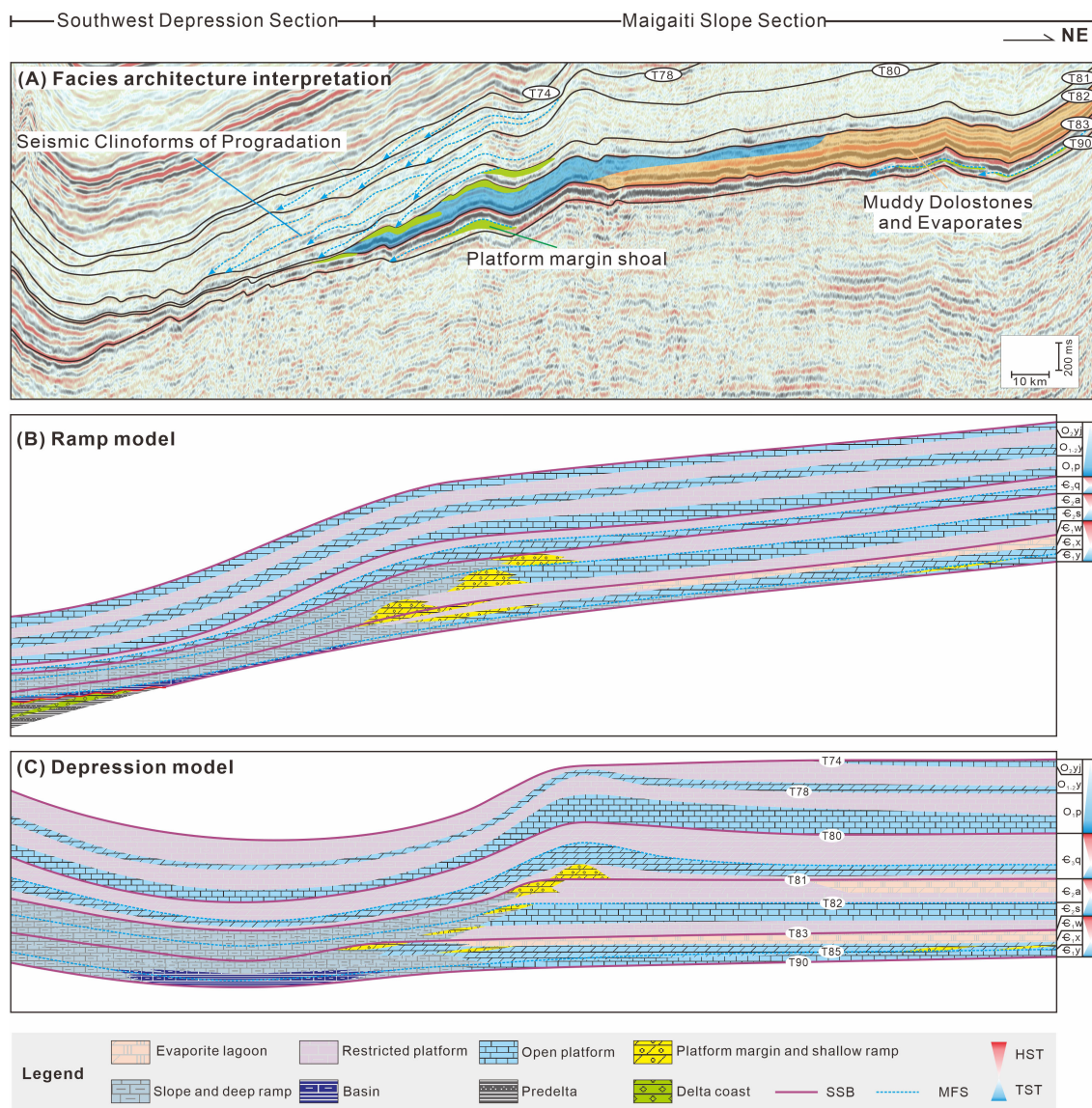


FIGURE 12 Facies architecture interpretation (A), ramp and depression sedimentary models (B, C) of the Lower Paleozoic strata in the southwestern Tarim Basin.

shoreline fluctuated near the center of the present Southwest Depression section in the late Ediacaran period, and coastal delta deposits developed to the south. Here, the earliest Cambrian transgression elevated the sea level drastically, and the coastal environment changed into the basin. During the subsequent Early and Middle Cambrian, the basin shallowed and evolved into a deep ramp and shelf slope. In the Ordovician, it turned into alternate open platforms and vertically restricted platforms (Figure 12B). In the depression model, the Lower Paleozoic strata deposited on the deep depression and the surrounding slopes. In the early Cambrian (E_{1y}), the central part of the Southwest Depression was a deep basin environment, which inherited from the Precambrian rift toudg. The southern slope was steep relative to the northern slope so voluminous sediments accumulated at the lower slope. During the highestand periods of the Early-Middle Cambrian (E_{1x}, E_{1w} and

E_{2a}), sediment was shed into the depression gradually, then the depression disappeared from the late Cambrian (Figure 12C).

Seismic clinoforms in the shelf break record the evolution of platforms. Analyses of clinoform structures revealed that tectonics, eustasy, climate, ecology, monsoons, and ocean currents have the potential to drive platform evolution from ramps to rimmed shelves (Lukasik and Simo, 2008). Among them, monsoons and ocean currents are able to steepen the platform margins, but because of their obvious directionality and regionality, they often form asymmetrical stratigraphic stacking patterns on different sides of platforms and grabens (Dorobek, 2008; Mulder et al., 2012; Betzler et al., 2014; Qin et al., 2022). However, the same ramp to rimmed shelf evolution is also seen in the southwest, northeast, and northwest of the Tarim Block (Gao and Fan, 2015; Wei et al., 2021). This shows that monsoons and ocean currents may not be

the dominant influence on the evolution of the carbonate platform here. Tectonic overload and rapid lithification of microbialites were proposed to have the potential to steepen shelf margins (Kenter et al., 2005; Bahamonde et al., 2007). But this is not the case in the southwest Tarim Basin. Previous studies proposed that the Cambrian-Ordovician epoch was a period of tectonic stability for the Tarim Block (Zhu et al., 2021b; Ma et al., 2022); while there were no metazoan reefs in the Early and Middle Cambrian, and the high-energy facies belt in the Early Cambrian was still dominated by microbialites (Ni et al., 2017; Bai et al., 2018). Therefore, tectonic compression and ecological changes did not influence platform evolution either.

There is a strong linear correlation between the sea level height and the progression, aggradation, and slope angles of each foreset deposit during the Oligocene-Lower Miocene period in the Browse Basin (Tesch et al., 2018). When the sea level rises rapidly, the carbonate factories in the platform margin can keep up or catch up with the sea level, while deeper environments outside the shelf break fail to. Therefore, the rapid rise of sea level during the E_2s transgression may be the dominant influence on platform evolution.

Climate change may also contribute to the transformation of carbonate platform morphology (Reijmer, 2021). But its contribution seems complicated. Climate warming and aridity were suggested to have caused the platform evolution from ramp to rimmed shelf at the Miocene carbonate margin of the North West Shelf, Australia (Riera et al., 2023). Furthermore, climate cooling can reduce the highstand sediment shedding to the slope by reducing the production rate of shallow marine carbonate factories, increasing the slope angle, and finally causing the transition from ramp to rimmed shelf (Colpaert et al., 2007). During the Early and Middle Cambrian, the Tarim Block migrated from high latitudes to the equator, and the climate gradually warmed (Zhao et al., 2018). However, seismic profiles in the study area show that no obvious reflections of platform margin features were observed when the first evaporite strata (E_{1w}) were deposited. On the contrary, obvious platform margin reflections appeared in the humid sequence (E_{2s}), sandwiched between two arid sequences (E_{1w} and E_{2a}). This suggests that the climate was already warming and drying before the ramp to rimmed shelf transition occurred in the Southwest Tarim Basin.

6 Conclusions

1. The Lower Paleozoic strata in the southwest Tarim Basin display vertical seismic amplitude differences: the high-amplitude reflections of the Lower-Middle Cambrian and low-amplitude reflections from Upper Cambrian to Middle Ordovician. The thickness of high-amplitude reflections is thinnest at the center of the Southwest Depression section and thickens to the north and south sides. Clinofolds in

high-amplitude reflections terminate upward together at the top reflector.

2. Seismic interpretation varies depending on the chronostratigraphic attributions of the southern high-amplitude reflections. If the southern high-amplitude reflections are attributed to the Cambrian strata, the thinnest reflection location was the top of the paleo-uplift or the center of the paleo-depression, and the thickened reflections to both sides were foresets; if attributed to the uppermost Ediacaran strata, the sedimentary background was a ramp dipping southward, and the northern reflection terminations within the high-amplitude reflections indicate retrograding high-energy buildups.
3. The seismic forward modeling results show different reflection characteristics of different sedimentary systems in hypothetical uplift, ramp, and depression models, which were then compared with real seismic reflections. The uplift interpretation was excluded, while the ramp and depression interpretations were potential paleo-topographic setting candidates. Finally, sedimentary models in the ramp and depression settings were tentatively established. The transition from an Early Cambrian carbonate ramp to a Middle Cambrian rimmed shelf was driven by a rapid rise in sea level and possible climate warming and aridity, which led to the building-up and retreat of the platform margin and backstepping foresets in the Maigaiti Slope section.

Data availability statement

The original contributions presented in the study are included in the article/supplementary material. Further inquiries can be directed to the corresponding author.

Author contributions

JL: Conceptualization, Data curation, Formal Analysis, Investigation, Methodology, Resources, Software, Validation, Visualization, Writing – original draft, Writing – review & editing. ZC: Funding acquisition, Investigation, Resources, Writing – review & editing. FG: Funding acquisition, Investigation, Resources, Writing – review & editing. SY: Conceptualization, Funding acquisition, Investigation, Methodology, Resources, Visualization, Writing – review & editing. XS: Data curation, Funding acquisition, Investigation, Methodology, Project administration, Resources, Visualization, Writing – review & editing. ML: Data curation, Funding acquisition, Investigation, Methodology, Resources, Writing – review & editing. SW: Data curation, Methodology, Software, Writing – review & editing. YCL: Investigation, Project administration, Resources, Visualization, Writing – review & editing. YBL: Resources, Writing – review & editing. DT: Investigation, Software, Writing – review & editing. ZZ: Investigation, Writing – review & editing. FH: Resources, Supervision, Writing – review & editing.

Funding

The author(s) declare financial support was received for the research, authorship, and/or publication of this article. This research was financially supported by the National Natural Science Foundation of China (Grant NO. 42002170) and SINOPEC (Grant NO. P24246).

Acknowledgments

Thanks are given to the Editor Chaojin Lu for many useful and constructive discussions and thorough revisions.

Conflict of interest

Authors ZC, FG, SY, XS, and ML were employed by Sinopec Northwest Oil Field Company. Author SW was employed by the company China Oilfield Services Limited.

The remaining authors declare that the research was conducted in the absence of any commercial or financial relationships that could be construed as a potential conflict of interest.

References

- Bahamonde, J. R., Merino-Tomé, O. A., and Heredia, N. (2007). A Pennsylvanian microbial boundstone-dominated carbonate shelf in a distal foreland margin (Picos de Europa Province, NW Spain). *Sediment. Geol.* 198, 167–193. doi: 10.1016/j.sedgeo.2006.12.004
- Bai, Y., Luo, P., Liu, W., Zhai, X. F., and Zhou, C. M. (2018). Characteristics and main controlling factors of microbial carbonate reservoir: a case study of upper member of Lower Cambrian Xiaerbulake Formation in Akesu area, Tarim Basin. *China Petrol. Explor.* 23, 95–107. doi: 10.3969/j.issn.1672-7703.2018.04.011
- Betzler, C., Lindhorst, S., Eberli, G. P., Lüdmann, T., Möbius, J., Ludwig, J., et al. (2014). Periplatform drift: the combined result of contour current and off-bank transport along carbonate platforms. *Geology* 42, 871–874. doi: 10.1130/G35900.1
- Bover-Arnal, T., Salas, R., Moreno-Bedmar, J. A., and Bitzer, K. (2009). Sequence stratigraphy and architecture of a late Early–Middle Aptian carbonate platform succession from the western Maestrat Basin (Iberian Chain, Spain). *Sediment. Geol.* 219, 280–301. doi: 10.1016/j.sedgeo.2009.05.016
- Campbell, A. E. (2005). Shelf-geometry response to changes in relative sea level on a mixed carbonate–siliciclastic shelf in the Guyana Basin. *Sediment. Geol.* 175, 259–275. doi: 10.1016/j.sedgeo.2004.09.003
- Cao, Z. C., Xu, Q. Q., Yu, T. X., Qin, H., Geng, F., Hao, J. L., et al. (2021). Significance of secondary hydrocarbon generation and crude oil cracking in paleo-reservoirs to hydrocarbon accumulation: A case study of cambrian source rocks in bachu-maigaiti area of tarim basin. *Xinjiang Petrol. Geol.* 42, 143–151. doi: 10.7657/XJPG20210203. (In Chinese with English abstract).
- Cathro, D. L., Austin, J. A. J., and Moss, G. D. (2003). Progradation along a deeply submerged Oligocene–Miocene heterozoan carbonate shelf: how sensitive are clinofolds to sea level variations? *AAPG Bull.* 87, 1547–1574. doi: 10.1306/05210300177
- Catuneanu, O., Abreu, V., Bhattacharya, J. P., Blum, M. D., Dalrymple, R. W., Eriksson, P. G., et al. (2009). Towards the standardization of sequence stratigraphy. *Earth Sci. Rev.* 92, 1–33. doi: 10.1016/j.earscirev.2008.10.003
- Chen, Y. Q., Yan, W., Han, C. W., Yang, P. F., and Li, Z. (2015). Redefinition on structural paleogeography and lithofacies paleogeography framework from Cambrian to Early Ordovician in the Tarim Basin: A new approach based on seismic stratigraphy evidence. *Natural Gas Geosci.* 26, 1831–1845. doi: 10.11764/j.issn.1672-1926.2015.10.1831
- Colpaert, A., Pickard, N., Mienert, J., Henriksen, L. B., Rafaelsen, B., and Andreassen, K. (2007). 3D seismic analysis of an Upper Palaeozoic carbonate succession of the Eastern Finnmark Platform area, Norwegian Barents Sea. *Sediment. Geol.* 197, 79–98. doi: 10.1016/j.sedgeo.2006.09.001
- Cui, H. F., Liu, J. L., Tian, L., Liu, J., and Zhang, N. C. (2018). Palaeotectonic pattern at the end of Sinian and its hydrocarbon significance in the southwest depression of Tarim Basin. *China Petrol. Explor.* 23, 67–75. doi: 10.3969/j.issn.1672-7703.2018.04.008. (In Chinese with English abstract)
- Cui, H. F., Tian, L., Zhang, N. C., Liu, J., and Zhang, J. J. (2016). Distribution characteristics of the source rocks from Cambrian Yuertusi Formation in the Southwest Depression of Tarim Basin. *Natural Gas Geosci.* 27, 577–583. doi: 10.11764/j.issn.1672-1926.2016.04.0577
- Cunha, J. A. O., Córdoba, V. C., Soares, U. M., Sousa, D. C., and Vital, H. (2021). Evolution of shallow and deep-water deposits included in the regressive drift succession of the Potiguar Basin (Brazilian Equatorial Margin) during the Late Cretaceous to Holocene. *J. S. Am. Earth Sci.* 110, 103420. doi: 10.1016/j.jsames.2021.103420
- Dorobek, S. L. (2008). “Tectonic and depositional controls on syn-rift carbonate platform sedimentation,” in *Controls on carbonate platform and reef development*. Eds. J. Lukask and J. A. Simo (Tulsa, Oklahoma, U. S. A.: SEPM Special Publication No. 89), 57–81.
- Espejel, R. L., Alves, T. M., and Martins-Ferreira, M. A. C. (2021). Depositional and geomorphic patterns of mixed calciclastic-siliciclastic systems on a deep-water Equatorial Margin. *Basin Res.* 33, 3321–3347.
- Feary, D. A., and James, N. P. (1995). Cenozoic biogenic mounds and buried Miocene(?) barrier reef predominantly cool-water carbonate continental margin — Eucla basin western Great Aust. *Bight. Geology* 23, 427–430.
- Feng, X. K., Liu, Y. B., Han, C. W., Yan, W., Dong, L., and He, Y. F. (2015). Development characteristics of Sinian rift in Tarim Basin and its significance for petroleum exploration. *Petrol. Geol. Engin.* 29, 5–10. doi: 10.3969/j.issn.1673-8217.2015.02.002
- Gao, Z. Q., and Fan, T. L. (2014). Intra-platform tectono-sedimentary response to geodynamic transition along the margin of the Tarim Basin, NW China. *J. Asian Earth Sci.* 96, 178–193. doi: 10.1016/j.jseas.2014.08.023
- Gao, Z. Q., and Fan, T. L. (2015). Carbonate platform-margin architecture and its influence on Cambrian–Ordovician reef-shoal development, Tarim Basin, NW China. *Mar. Petrol. Geol.* 68, 291–306. doi: 10.1016/j.marpetgeo.2015.08.033
- Gao, Y. F., Fu, H., Wang, T., Yang, H. F., and Zhao, L. X. (2015). The features of Ordovician sequence boundaries and its controls on carbonate karst in Tarim Basin. *Xinjiang Geol.* 33, 362–367. doi: 10.3969/j.issn.1000-8845.2015.03.015
- Gao, Z. Q., Shi, J. Y., Lv, J. L., and Chang, Z. (2022). High-frequency sequences, geochemical characteristics, formations, and distribution predictions of the lower Cambrian Yuertusi Formation in the Tarim Basin. *Mar. Petrol. Geol.* 146, 105966. doi: 10.1016/j.marpetgeo.2022.105966
- Geng, F., Su, B. R., Hao, J. L., Fan, W. F., and Duan, X. (2023). The Cambrian sedimentary sequences and paleogeographic evolution in the Bachu-Maigaiti area,

- southwestern Tarim Basin. *Sediment. Geol. Tethyan Geol* 43, 856–870. doi: 10.19826/j.cnki.1009-3850.2022.04013
- Gong, C. L., Steel, R. J., Wang, Y. M., Lin, C. S., and Olariu, C. (2016). Grain size and transport regime at shelf edge as fundamental controls on delivery of shelf-edge sands to deepwater. *Earth-Sci. Rev.* 157, 32–60. doi: 10.1016/j.earscirev.2016.04.002
- Gradstein, F. M., Ogg, J. G., Schmitz, M. D., and Ogg, G. M. (2020). *Geologic Time Scale 2020* (Amsterdam, Netherlands: Elsevier), 1349p.
- Grant, R. J., Underhill, J. R., Hernández-Casado, J., Baker, S. M., and Jamieson, R. J. (2018). Upper Permian Zechstein Supergroup carbonate-evaporite platform palaeomorphology in the UK Southern North Sea. *Mar. Petrol. Geol.* 100, 484–518. doi: 10.1016/j.marpetgeo.2017.11.029
- Haq, B. U., and Schutter, S. R. (2008). A chronology of Paleozoic sea-level changes. *Science* 322, 64–59. doi: 10.1126/science.1161648
- He, D. F., Jia, C. Z., De, S., Zhang, C. J., Meng, Q. R., Shi, X., et al. (2005). Formation and evolution of polycyclic superimposed Tarim Basin. *Oil Gas Geology* 26, 64–77. doi: 10.3321/j.issn:0253-9985.2005.01.010
- He, D. F., Jia, C. Z., Zhao, W. Z., Xu, F. Y., Luo, X. R., and Liu, W. H. (2023). Research progress and key issues of ultra-deep oil and gas exploration in China. *Petrol. Explor. Dev.* 50, 1162–1172. doi: 10.1016/S1876-3804(24)60470-2
- He, Y. W., Kerans, C., Zeng, H. L., Janson, X., and Scott, S. Z. (2019). Improving three-dimensional high-order seismic-stratigraphic interpretation for reservoir model construction: an example of geostatistical and seismic forward modeling of Permian San Andres shelf-Grayburg platform mixed clastic-carbonate strata. *AAPG Bull.* 103, 1839–1887. doi: 10.1306/11211817244
- He, J. Y., Wu, G. H., Xu, B., Qu, T. L., Li, H. H., and Cao, Y. H. (2010). Characteristics and petroleum exploration significance of unconformity between Sinian and Cambrian in Tarim Basin. *Chin. J. Geol.* 45, 698–706. doi: 10.3969/j.issn.0563-5020.2010.03.006
- Hunt, D., and Tucker, M. E. (1992). Stranded parasequences and the forced regressive wedge systems tract deposition during base-level fall. *Sediment. Geol.* 81, 1–9. doi: 10.1016/0037-0738(92)90052-5
- Janson, X., Eberli, G. P., Bonnaffé, F., Gaumet, F., and Casanove, V. D. (2007). Seismic expressions of a Miocene prograding carbonate margin, Mut Basin, Turkey. *AAPG Bull.* 91, 685–713. doi: 10.1306/11020605192
- Janson, X., Kerans, C., Loucks, R., Marhx, M. A., Reyes, C., and Murguía, F. (2011). Seismic architecture of a Lower Cretaceous platform-to-slope system, Santa Agueda and Poza Rica fields, Mexico. *AAPG Bull.* 95, 105–146. doi: 10.1306/06301009107
- Jia, C. Z. (1997). *Tectonic Characteristics and Petroleum, Tarim Basin* (China: Beijing, China: Petroleum Industry Press), 295p (in Chinese).
- Jin, Z. J., and Wang, Q. C. (2004). New progress in the study of typical superimposed basins and hydrocarbon accumulation in China-A case study of tarim basin. *Sci. China Ser. D Earth Sci.* 34, 1–12. doi: 10.3321/j.issn:1006-9267.2004.z1.001
- Kenter, J. A. M., Harria, P. M., and Porta, G. D. (2005). Steep microbial boundstone-dominated platform margins—examples and implications. *Sediment. Geol.* 178, 5–30. doi: 10.1016/j.sedgeo.2004.12.033
- Lee, G. H., and Watkins, J. S. (1998). Seismic sequence stratigraphy and hydrocarbon potential of the phu khanh basin, offshore Central Vietnam, South China sea. *AAPG Bull.* 82, 1711–1735.
- Li, K. (2009). *The Three Main Paleohigh's Evolution and Affection Hydrocarbon Accumulation, Tarim Basin* (Chengdu, China: Chengdu University of Technology), 169p.
- Li, S. M., Amrani, A., Pang, X., Yang, H. J., Said-Ahmad, W., Zhang, B. S., et al. (2015). Origin and quantitative source assessment of deep oils in the Tazhong Uplift, Tarim Basin. *Org. Geochem.* 78, 1–22. doi: 10.1016/j.orggeochem.2014.10.004
- Lin, S. C., Fu, H., and Zeng, Y. (2014). Recognition and the character of sequence boundary of Ordovician in Yubei area of Tarim Basin. *Xinjiang Geology* 32, 219–224. doi: 10.3969/j.issn.1000-8845.2014.02.015
- Lin, B., Zhang, X., Xu, X., Yuan, J. Y., Neng, Y., Zhu, J. W., et al. (2015). Features and effects of basement faults on deposition in the Tarim basin. *Earth-Sci. Rev.* 145, 43–55. doi: 10.1016/j.earscirev.2015.02.008
- Liou, J. G., Graham, S. A., Maruyama, S., and Zhang, R. Y. (1996). Characteristics and tectonic significance of the late Proterozoic Aksu blueschists and diabasic dikes northwest Xinjiang, China. *Inter. Geol. Rev.* 38, 228–244.
- Liu, H., Somerville, I. D., Lin, C. S., and Zuo, S. J. (2016). Distribution of Palaeozoic tectonic superimposed unconformities in the Tarim Basin, NW China: significance for the evolution of palaeogeomorphology and sedimentary response. *Geol. J.* 51, 627–651. doi: 10.1002/gj.v51.4
- Lu, X. B., Wang, Y., Tian, F., Li, X. H., Yang, D. B., Li, T., et al. (2017). New insights into the carbonate karstic fault system and reservoir formation in the Southern Tahe area of the Tarim Basin. *Mar. Petrol. Geol.* 86, 587–605. doi: 10.1016/j.marpetgeo.2017.06.023
- Lukasik, J., and Simo, J. A. (2008). “Controls on development of Phanerozoic carbonate platforms and reefs—introduction and synthesis,” in *Controls on carbonate platform and reef development*. Eds. J. Lukasik and J. A. Simo (Tulsa, Oklahoma, U.S.A.: SEPM Special Publication No. 89), 5–12.
- Lv, H. T., Zhang, Z. P., Shao, Z. B., Zhang, G. F., and Yue, Y. (2010). Structural evolution and exploration significance of the Early Paleozoic palaeouplifts in Bachu-Maigaiti area, the Tarim Basin. *Oil&Gas Geol* 31, 76–83. doi: 10.11743/ogg20100113. (In Chinese with English abstract)
- Ma, B. S., Tian, W. Z., and Wu, G. H. (2022). The subduction-related Great Unconformity in the Tarim intracraton, NW China. *Global Planetary Change* 215, 103883. doi: 10.1016/j.gloplacha.2022.103883
- Mulder, T., Ducassou, E., Eberli, G. P., Hanquiez, V., Gonthier, E., Kindler, P., et al. (2012). New insights into the morphology and sedimentary processes along the western slope of Great Bahama Bank. *Geology* 40, 603–606. doi: 10.1130/G32972.1
- Mulder, T., Joumes, M., Hanquiez, V., Gillet, H., Reijmer, J. J. G., Tournadour, E., et al. (2017). Carbonate slope morphology revealing sediment transfer from bank-to-slope (Little Bahama Bank, Bahamas). *Mar. Petrol. Geol.* 83, 26–34. doi: 10.1016/j.marpetgeo.2017.03.002
- Ni, X. F., Huang, L. L., Chen, Y. Q., Zheng, J. F., Xiong, Y. X., Zhu, Y. J., et al. (2017). Characteristics and main controlling factors of the Cambrian pre-salt dolomite reservoirs in Tazhong Block, Tarim Basin. *Oil Gas Geol* 38, 489–498. doi: 10.11743/ogg20170308
- Playton, T. E., and Kerans, C. (2015). Late Devonian carbonate margins and foreslopes of the Lennard shelf, Canning Basin, western Australia, part A: development during backstepping and the aggradation-to-progradation transition. *J. Sediment. Res.* 85, 1334–1361. doi: 10.2110/jsr.2015.84
- Principaud, M., Mulder, T., Gillet, H., and Borgomano, J. (2015). Large-scale carbonate submarine mass-wasting along the northwestern slope of the Great Bahama Bank (Bahamas): morphology, architecture, and mechanisms. *Sediment. Geol.* 317, 27–42. doi: 10.1016/j.sedgeo.2014.10.008
- Qian, Y. X., Wang, L., Kang, Z. H., Chen, Y., Jia, C. S., Tian, M., et al. (2018). Detrital geochemistry studies on the Malieziken group of ordocivian in Southwestern Tarim. *Xinjiang Geol* 36, 30–37. doi: 10.3969/j.issn.1000-8845.2018.01.005
- Qin, Y. P., Wu, S. G., and Betzler, C. (2022). Backstepping patterns of an isolated carbonate platform in the northern South China Sea and its implication for paleoceanography and paleoclimate. *Mar. Petrol. Geol.* 146, 105927. doi: 10.1016/j.marpetgeo.2022.105927
- Rankey, E. C. (2017). Seismic architecture and seismic geomorphology of heterozoan carbonates: Eocene-Oligocene, Browse Basin, Northwest Shelf, Australia. *Mar. Petrol. Geol.* 82, 424–443. doi: 10.1016/j.marpetgeo.2017.02.011
- Reijmer, J. J. G. (2021). Marine carbonate factories: Review and update. *Sedimentology* 68, 1729–1796. doi: 10.1111/sed.12878
- Riera, R., Paumard, V., and Bourget, J. (2023). Evolution of the Exmouth-Barrow carbonate margin through the Miocene: Insights from 3D seismic data and field investigations (North West Shelf, Australia). *Sediment. Geol.* 449, 106371. doi: 10.1016/j.sedgeo.2023.106371
- Rinke-Hardkopf, L., Reuning, L., Bourget, J., and Back, S. (2018). Syn-sedimentary deformation as a mechanism for the initiation of submarine gullies on a carbonate platform to slope transition. *Browse Basin Aust. North West Shelf. Mar. Petrol. Geol.* 91, 622–630. doi: 10.1016/j.marpetgeo.2017.12.034
- Saller, A. H., Walden, S., Robertson, S., Nims, R., Schwab, J., Hagiwara, H., et al. (2004). “Three-dimensional seismic imaging and reservoir modeling of an upper Paleozoic “reefal” buildup, Reinecke field, west Texas, United States,” in *Seismic Imaging of Carbonate Reservoirs and Systems*, vol. 81. Eds. G. P. Eberli, J. L. Masaferrero and J. F. Sarg (Tulsa, Oklahoma, U.S.A.: AAPG Memoir), 107–122.
- Schlager, W. (1998). “Exposure, drowning and sequence boundaries on carbonate platforms,” in *Reefs and carbonate platforms of the W Pacific and Indian Oceans*, vol. 25. Eds. G. Camoin and P. Davies (Tulsa: SEPM—Society for Sedimentary Geology: IAS Special Publication), 3–21. SEPM—Society for Sedimentary Geology.
- Seyedmehdi, Z., George, A. D., and Tucker, M. E. (2016). Sequence development of a latest Devonian-Tournaisian distally-steepened mixed carbonate-siliciclastic ramp, Canning Basin, Australia. *Sediment. Geol.* 333, 164–183. doi: 10.1016/j.sedgeo.2015.12.012
- Tesch, P., Reece, R. S., Pope, M. C., and Markello, J. R. (2018). Quantification of architectural variability and controls in an Upper Oligocene to Lower Miocene carbonate ramp, Browse Basin, Australia. *Mar. Petrol. Geol.* 91, 432–454. doi: 10.1016/j.marpetgeo.2018.01.022
- Tian, J., Wu, S. G., Lv, F. L., Wang, D., Wang, B., Zhang, X., et al. (2015). Middle Miocene mound-shaped sediment packages on the slope of the Xisha carbonate platforms, South China Sea: Combined result of gravity flow and bottom current. *Elsevier logo. Deep Sea Res. Part II: Topical Stud. Oceanography* 122, 172–184.
- Tian, L., Zhang, H. Q., Liu, J., Zhang, N. C., and Shi, X. Q. (2020). Distribution of Nanhua-Sinian rifts and proto-type basin evolution in southwestern Tarim Basin, NW China. *Petrol. Explor. Dev.* 47, 1122–1133. doi: 10.1016/S1876-3804(20)60130-1
- Vail, P. R., Mitchum, R. M. Jr., and Thompson, S. I. I. (1977). “Seismic stratigraphy and global changes of sea level, Part 4: global cycles of relative changes of sea level,” in *Seismic Stratigraphy - Applications to Hydrocarbon Exploration* vol. 26. Ed. C. E. Payton (Tulsa, Oklahoma, U.S.A.: AAPG Memoir), 83–97.
- Vecsei, A., and Sanders, D. G. K. (1997). Sea-level highstand and lowstand shedding related to shelf margin aggradation and emersion, Upper Eocene-Oligocene of Maiella carbonate platform, Italy. *Sediment. Geol.* 112, 219–234. doi: 10.1016/S0037-0738(97)00044-4
- Wang, Z. M., Xie, H. W., Chen, Y. Q., Qi, Y. M., and Zhang, K. (2014). Discovery and exploration of Cambrian subsalt dolomite original hydrocarbon reservoir at zhongshen-1 well in Tarim Basin. *China Petrol. Explor.* 19, 1–13. doi: 10.3969/j.issn.1672-7703.2014.02.001
- Wei, G. Q., Zhu, Y. J., Zheng, J. F., Yu, G., Ni, X. F., Yan, L., et al. (2021). Tectonic lithofacies paleogeography, large-scale source-reservoir distribution and exploration

zones of Cambrian subsalt formation, Tarim Basin, NW China. *Petrol. Explor. Dev.* 48, 1–13. doi: 10.1016/S1876-3804(21)60287-2

Wu, L., Guan, S. W., Ren, R., Wang, X. B., Yang, H. J., Jin, J. Q., et al. (2016). The characteristics of Precambrian sedimentary basin and the distribution of deep source rock: A case study of Tarim Basin in Neoproterozoic and source rocks in Early Cambrian, Western China. *Petrol. Explor. Dev.* 43, 988–999. doi: 10.1016/S1876-3804(16)30116-1

Wu, G. H., Xiao, Y., Bonin, B., Ma, D. B., Li, X., and Zhu, G. Y. (2018). Ca. 850 Ma magmatic events in the Tarim Block: age, geochemistry and implications for assembly of Rodinia supercontinent. *Precam. Res.* 305, 489–503. doi: 10.1016/j.precamres.2017.10.020

Wu, L., Zhu, G. Y., Yan, L., Feng, X. Q., and Zhang, Z. Y. (2021). Late Ediacaran to Early Cambrian tectonic–sedimentary controls on Lower Cambrian black shales in the Tarim Basin, Northwest China. *Global Planet. Change* 205, 103612. doi: 10.1016/j.gloplacha.2021.103612

Xu, X., Chen, H. L., Zuza, A. V., Yin, A., Yu, P., Lin, X. B., et al. (2023). Phanerozoic cratonization by plume welding. *Geology* 51, 209–214. doi: 10.1130/G50615.1

Xu, Z. Q., He, B. Z., Zhang, C. L., Zhang, J. X., Wang, Z. M., and Cai, Z. H. (2013). Tectonic framework and crustal evolution of the Precambrian basement of the Tarim Block in NW China: new geochronological evidence from deep drilling samples. *Precam. Res.* 235, 150–162. doi: 10.1016/j.precamres.2013.06.001

Yang, X., Li, H. L., Yue, Y., Liu, S. L., Li, J. J., Xiong, P., et al. (2017). The strata and palaeo-geomorphology framework at the end of Neoproterozoic and development mode of source rocks at the beginning of Cambrian. *Nat. Gas Geosci* 28, 189–198. doi: 10.1016/j.jnggs.2018.02.003

Yang, Y. J., Liu, J. D., Tian, J. C., Meng, W. B., and Zhu, H. (2011). The Cambrian sequence stratigraphy framework and source-reservoir-cap rock association of Bachu uplift in Tarim Basin. *J. Southwest Petrol. Univer. (Science Technol. Edition)* 33, 53–58. doi: 10.3863/j.issn.1674-5086.2011.04.009

Yang, H. J., Wu, G. H., Kuskuy, T. M., Chen, Y. Q., and Xiao, Y. (2018). Paleoproterozoic assembly of the North and South Tarim terranes: new insights from deep seismic profiles and Precambrian granite cores. *Precam. Res.* 305, 489–503. doi: 10.1016/j.precamres.2017.11.015

Yin, A., and Nie, S. (1996). “A Phanerozoic palinspastic reconstruction of China and its neighboring regions,” in *The Tectonics of Asia*. Eds. A. Yin and T. M. Harrison (Cambridge University Press, New York), 442–485.

Yuan, H. W., Chen, S., Dai, K., Guo, X. C., Kong, L. H., Feng, N. N., et al. (2022). Distribution of Cambrian source rock controlled by the inherited paleotopography on the Precambrian basement in the Tarim Basin, NW China. *Front. Earth Sci.* 10, 864082. doi: 10.3389/feart.2022.864082

Yue, Y., and Luo, S. H. (2019). Structural characteristics and their control over Ordovician hydrocarbon migration pathway system in Yubei Area, Tarim Basin. *Geol. Sci. Technol. Inf* 38, 20–30. doi: 10.19509/j.cnki.dzqk.2019.0502 (in Chinese with English abstract).

Zeng, H. L., Henry, S. C., and Riola, J. P. (1998). Stratal slicing, part II: real seismic data. *Geophysics* 63, 514–522. doi: 10.1190/1.1444352

Zeng, H. L., and Hentz, T. F. (2004). High-frequency sequence stratigraphy from seismic sedimentology: applied to Miocene, Vermilion Block 50, Tiger Shoal area, offshore Louisiana: *AAPG Bull.* 88, 153–174. doi: 10.1306/10060303018

Zeng, H. L., Loucks, R., Janson, X., Wang, G. Z., Xia, Y. P., Yuan, B. H., et al. (2011). Three-dimensional seismic geomorphology and analysis of the Ordovician paleokarst drainage system in the central Tabei Uplift, northern Tarim Basin, western China. *AAPG Bull.* 95, 2061–2083. doi: 10.1306/03111110136

Zeng, H. L., Xu, Z., Liu, W., Janson, X., and Fu, Q. L. (2022). Seismic-informed carbonate shelf-to-basin transition in deeply buried Cambrian strata, Tarim Basin, China. *Mar. Petrol. Geol.* 136, 105448. doi: 10.1016/j.marpetgeo.2021.105448

Zhang, F. Q., Dilek, Y., Cheng, X. G., Wu, H. X., Lin, X. B., and Chen, H. L. (2019). Late Neoproterozoic–early Paleozoic seismic structure–stratigraphy of the SW Tarim Block (China), its passive margin evolution and the Tarim–Rodinia breakup. *Precam. Res.* 334, 105456. doi: 10.1016/j.precamres.2019.105456

Zhang, X. L., Gao, Z. Q., Maselli, V., and Fan, T. L. (2023). Tectono-sedimentary characteristics and controlling factors of the lower-middle Cambrian gypsum-salt rocks in the Tarim Basin, Northwest China. *Mar. Petrol. Geol.* 151, 106189. doi: 10.1016/j.marpetgeo.2023.106189

Zhang, S. C., Huang, H., Su, J., Liu, M., and Zhang, H. F. (2014). Larter, Geochemistry of Paleozoic marine oils from the Tarim Basin, NW China. Part 4: Paleo-biodegradation and oil charge mixing. *Org. Geochem.* 67, 41–57.

Zhao, P., He, J., Deng, C., Chen, Y., and Mitchell, R. N. (2021). Early Neoproterozoic (870–820 Ma) amalgamation of the Tarim craton (northwestern China) and the final assembly of Rodinia. *Geology* 49, 1277–1282. doi: 10.1130/G48837.1

Zhao, Z. J., Luo, J. H., Zhang, Y. B., Wu, X. N., and Pan, W. Q. (2011). Lithofacies paleogeography of Cambrian sequences in the Tarim Basin. *Acta Petrol. Sin.* 32, 937–947. doi: 10.7623/syxb201106003

Zhao, G. C., Wang, Y. J., Huang, B. C., Dong, Y. P., Li, S. Z., Zhang, G. W., et al. (2018). Geological reconstructions of the East Asian blocks: From the breakup of Rodinia to the assembly of Pangea. *Earth-Sci. Rev.* 186, 262–286. doi: 10.1016/j.earscirev.2018.10.003

Zheng, X. L. (2016). *The fault characteristics and paleo- uplift migration of Bachu uplift, Tarim Basin* (Hangzhou, Zhejiang, China: Zhejiang University), 118pp. (In Chinese with English abstract).

Zhu, G. Y., Chen, F. R., Chen, Z. Y., Zhang, Y., Xing, X., Tao, X. W., et al. (2016). Discovery and basic characteristics of the high-quality source rocks of the Cambrian Yuertusi Formation in Tarim Basin. *J. Nat. Gas Geosci* 27, 8–21. doi: 10.1016/j.jnggs.2016.05.002

Zhu, G. Y., Liu, W., and Wu, G. H. (2021b). Geochemistry and U-Pb-Hf detrital zircon geochronology of metamorphic rocks in terranes of the West Kunlun Orogen: Protracted subduction in the northernmost Proto-Tethys Ocean. *Precamb. Res.* 363, 106344. doi: 10.1016/j.precamres.2021.106344

Zhu, Y. J., Zheng, J. F., Gao, P., Qiao, Z. F., Yu, G., Liu, L. L., et al. (2021a). Tectonic-lithofacies paleogeography and sizeable reservoir potential in the early cambrian postrift depressed carbonate ramp, Tarim Basin, NW China. *Lithosphere*, 2021, 8804537. doi: 10.2113/2021/8804537

Zuza, A. V., and Yin, A. (2017). Balkatach hypothesis: A new model for the evolution of the Pacific, Tethyan, and Paleo-Asian oceanic domains. *Geosphere* 13, 1664–1712. doi: 10.1130/GES01463.1